Transient temperature fields and thermal actions in the Leaning Tower of Pisa

Maurizio Froli
Enrico Ulivieri

Statistical analysis of temperature measurements in the Leaning Tower of Pisa in comparison with theoretical predictions

Maurizio Froli
Paolo Formichi

The calculation of thermal movements and eigenstresses in the Leaning Tower of Pisa

Maurizio Froli
Enrico Ulivieri

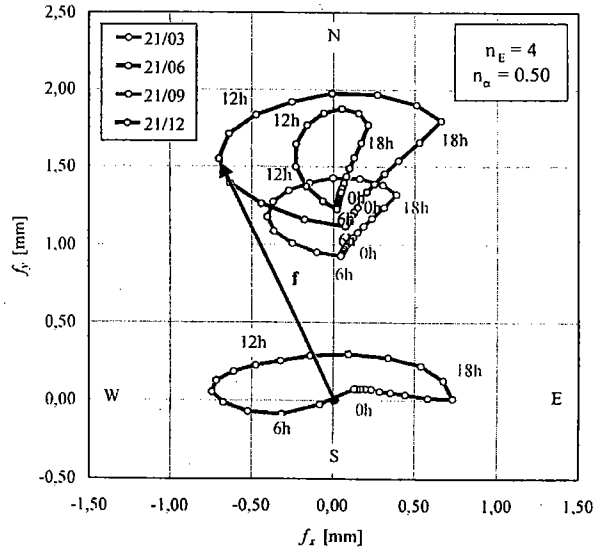

Maurizio Froli
Enrico Ulivieri

Transient temperature fields and thermal actions in the Leaning Tower of Pisa

Based on the analytical description of the daily variations of the main meteorological agents all over an idealised, mean meteorological year and taking also into account shadowing effects, a complete yearly transient study of the thermal response of the Tower of Pisa is performed.

The model describes the hourly evolution of the temperature fields in the basement, in the shaft and in the columns of the monument at any day of the idealised year.

The theoretical knowledge of the punctual time and space variation of the temperature fields over the cross sections of the Tower allows the calculation of synthesis quantities like the Effective Mean Temperature and the Effective Global Linear Gradient which constitute the bases to predict thermal movements and eigenstresses.

Instationäre Temperaturfelder und thermische Einwirkungen auf den Schiefen Turm von Pisa. *Auf der Basis einer rechnerischen Erfassung der täglichen Veränderungen der wichtigsten meteorologischen Einflüsse, hochgerechnet auf ein idealisiertes meteorologisches Jahr einschließlich auftretender Verschattungseffekte wird eine Studie der instationären thermischen Reaktionen des Schiefen Turms von Pisa über einen kompletten Jahreszeitraum vorgelegt.*

Das Modell erlaubt die Erfassung der Temperaturfelder im Fundament, im Schaft und in den Säulen des Bauwerks im Stundentakt an allen Tagen eines idealisierten Jahres.

Mit Hilfe der theoretischen Grundlagen von Raum- und Zeitveränderungen der Temperaturfelder über die Querschnitte eines Bauteils lassen sich Beschreibungsgrößen wie die Effektive Haupttemperatur (E.M.T.) und der Effektive Global-Linear-Gradient (E.G.L.G.) berechnen, die die Basis für die einfache Vorhersage der Temperaturverformungen und Eigenspannungen liefern.

1 Introduction

Solar radiation, air temperature, wind and rain induce non-stationary and spatially non-linear temperature fields in the thickness of the walls of any masonry building. Movements as well as primary and secondary eigenstresses are the mechanical consequences of these nonuniform fields. Normally, neither the safety nor even the serviceability of common masonry buildings can be seriously compromised by thermal stresses since the development of micro-cracks over small areas is sufficient to attenuate them. The same problem attains on the contrary a considerable relevance in the case of monumental masonry buildings like the Leaning Tower of Pisa.

Micro-cracking and the periodic oscillation of thermal stresses may degrade, in conjunction with high gravity stresses, the integrity of the S. Giuliano marble facings, while the top of the Tower describes every day, under the effect of solar radiation, an ellipsis whose main half-diameter may have in some period of the year the same dimensions of the annual increment in slope that occurred due to the soil settlement before counterweights were applied in 1991 and underescavation was started in February 1999.

A reliable and as far as possible complete knowledge of the thermal behaviour of the Tower is therefore necessary, together with other informations, in order to check the serviceability and maintenance status of the masonry.

Indeed, already in 1967 the first temperature measurements were performed inside the walls of the Tower at the level of the 5th cornice by means of thermocouples embedded in two holes drilled in the north-south direction [1]. Since 1991 temperatures have been measured and recorded every hour by means of thermistors placed in the same holes and attention was also paid to the definition of the micro-climate around the Tower and to the measurements of masonry surface temperatures [2].

Nevertheless, a reliable structural analysis can be performed only if a complete mapping of the temperature fields within the structures of the fabric is available and this goal cannot be completely achieved experimentally since temperature measurements are necessarily taken in few points and are not sufficient to completely describe the complex physical phenomenon of the space and time variations of these fields. Experience must therefore be integrated with an adequate theoretical model able to give the hourly temperature distributions at any point of the principal parts of the structure and at each day of an idealised, average meteorological year.

The problem of calculating the temperature fields induced by strongly transient boundary interactions with the climatic agents of the Tower, which has an enormous thermal inertia and a very complicated external shape, is extremely complex. We decided to build up a calculation scheme refined enough to allow the nucleation of the dominant aspects of the thermal behaviour of the Tower but at the same time simple enough to allow reasonable numerical analysis since it is almost impossible, and at this stage of investigation perhaps even misleading, expecting to get the temperature distributions of every secondary detail which would have required a much bigger implementation of automatic calculation facilities than that used in the present study.

2 The model

2.1 Geometrical simplifications

In order to describe analytically the incoming direct solar radiation and the related shadowing effects, the complex geometry of the Tower had to be drastically simplified according to the following assumptions:

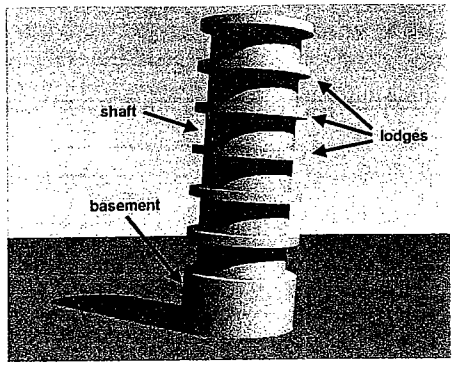

Fig. 1. The shape of the model
Bild 1. Modell

although slightly upwards curved, the axis of the Tower is supposed perfectly straight. The little angle comprised between the north-south direction and the plane of maximum inclination (~ 10°) is neglected.

Because of its light open-worked, unroofed structure the belfry is continuously and almost uniformly cooled down or warmed up by the climatic agents. For this reason and since it is located at the top of the Tower, it is assumed not to influence significantly the thermal response of the underlying parts of the structure.

The external surfaces are supposed perfectly smooth, without openings, decorations and other relieves. The columns of the lodges are assimilated to straight cylinders and the related complex of cross vaults, arcades and round walks has been schematized as cylindrical tora. Fig. 1 shows the resulting shape of the model. For sake of clearness the columns of the lodges are not represented.

2.2 Heat propagation hypotheses and materials properties

The temperature fields induced by the climatic agents into the Tower have been separately calculated for the basement, the shaft and the columns under the following simplifying assumptions.

The basement has been schematized as a hollow cylinder composed by three concentric circular cylindrical coronas (Fig. 4) which reproduce the outer marble facings and the intermediate infill masonry. As already said, the presence of the openings and of the stair case is neglected. The shaft has been schematized in an analogous way (Fig. 5).

The columns have been assimilated to solid cylinders thermally insulated at the ends.

For all the three problems it has been assumed that the heat fluxes along the axial direction are negligible in order to reduce them all to 2D problems governed, as known, by Fourier equations of the type

$$\frac{\partial^2 T}{\partial x^2} + \frac{\partial^2 T}{\partial y^2} = \frac{\rho C_p}{\lambda} \frac{\partial T}{\partial t} \quad (1)$$

where T is the temperature of the body, t is the time variable, x and y are centroidal axes respectively oriented along the E-W and the N-S direction, ρ is the density, C_p is the specific heat and λ is the coefficient of thermal conductivity of the constituent materials. In spite of the very large amount of tests that have been periodically performed on the white S. Giuliano marble of the facings and on the infill masonry [1], [3], no direct experimental data could be found on the thermal properties of such materials, except the density ρ. Appropriate specific heat C_p and thermal conductivity coefficients λ had therefore to be selected from literature data of similar materials and are given in Table 1 while mean values of the *Young*'s Modula are obtained from direct measurements on cylindrical specimens [3].

2.3 Boundary conditions

Convection and radiation heat exchanges take place between the surfaces of the Tower and the surrounding environment. If we neglect for sake of simplicity heat losses due to direct pouring rain and subsequent evaporation, the heat exchanged for unit surface, unit time is given by

$$q = q_c + q_{rs} + q_{ra} + q_{rt} + q_{re} \quad (2)$$

where q_c is the incoming or outgoing convection heat, q_{rs} is the incoming heat due to direct and diffusive solar radiation, q_{ra} is the incoming heat due to the thermal radiation of the atmosphere, q_{rt} is the incoming heat due to the thermal radiation of the soil and the surrounding buildings and q_{re} is the outgoing thermal radiation of the surface.

The heat exchanged through convection may be expressed by the *Newton*'s law of cooling:

$$q_c = \alpha (T_s - T_a) \quad (3)$$

where T_s is the surface temperature, T_a (°C) is the shade air temperature and α is the convection heat transfer coefficient. The exact determination of α is very problematic since it depends on a lot of variables including the unknown surface temperature and the turbulence degree of the surrounding air.

Table 1. Physical properties of the masonry materials
Tabelle 1. Physikalische Eigenschaften des Mauerwerks

	Material	C_p [J/Kg °K]	λ [W/m² °K]	ρ [Kg/m³]	E [MPa]
F	S. Giuliano marble facings	880	0.6862	2800	27610
I	Infill masonry	840	1.396	2000	7220 ÷ 6150

(F = facing, I = infill)

Usually, in similar analyses [4], α has been simply and successfully expressed just as function of the wind speed V [m/s] by the following empirical relation:

$$\alpha = 13.5 + 3.88\ V\ [W/m\,°C] \qquad (4)$$

In the present study the wind velocity has been assumed to be constant and equal to a mean value of 3.5 m/s for the outer surfaces and zero for the inner surface.

The incoming heat due to direct and diffusive solar radiation q_{rs} may be expressed as

$$q_{rs} = a\,(i + d) \qquad (5)$$

where a is the colour and roughness dependent absorption coefficient of the surface ($0 \le a \le 1$), here taken equal to 0.8; i is the component of the direct solar radiation perpendicular to the examined surface portion (W/m^2), strongly dependent on the angle that the incident sun rays form with the normal at the surface and on its shadow condition while d, diffuse solar radiation (W/m^2), is independent from these variables.

The ingoing heat fluxes due to the short wave thermal radiation of the atmosphere (q_{ra}), the soil and the surrounding buildings (q_{rt}), as well as the outgoing short wave thermal radiation of the surface (q_{re}) could be all expressed by the *Stefan-Boltzmann* law of the thermal radiation which contains the fourth powers of the air temperature and of the surface temperature, at first unknown [5].

These heat fluxes almost compensate each other in summer and may be therefore neglected. In winter, on the contrary, the outgoing re-irradiation plays an important role especially during cold and cloudless nights but, for sake of calculation simplicity, in order to avoid non-linearity in the boundary conditions, this term has been neglected also during this season. Likely analysis performed under the same hypotheses on massive concrete bridges [4] assured a good agreement between theoretical predictions and measurements.

A further simplification of the boundary condition can be made by reducing it to a pure convection heat exchange q_c between the surface at the temperature T_s and the surrounding air put at an equivalent temperature T_a^* [5]:

$$q_c = \alpha\,(T_s - T_a^*) \qquad (6)$$

with

$$T_a^* = T_a + T_i^* + T_d^* = T_a + a\,\frac{i}{\alpha} + a\,\frac{d}{\alpha} \qquad (7)$$

where T_i^* is the equivalent temperature due to the direct solar radiation and T_d^* is the equivalent temperature due to the diffuse solar radiation.

T_a^* is the ideal temperature that the air should reach in the neighbourhood of a surface portion for the entire local heat transfer to be reduced to a purely convective exchange, expressed by the *Newton*'s law of cooling.

T_a, T_d^* and T_i^* are all variable with time, but while T_a, T_d^* are with good approximation instantaneously uniform over a given surface even if it is curved, T_i^* depends on the orientation of the examined surface portion.

2.4 The mean meteorological year

The enormous thermal inertia of the Tower required that the transient heat transfer analysis was performed without interruptions through a entire representative meteorological year (see § 3). That implied that the polar variation of T_a^* all around the boundary surfaces of the basement, the shaft and the columns had to be known from hour to hour at all the days of one year, but since no direct in situ monitoring of i and d has been until now performed for so a long period, it was necessary to model it with a preliminary theoretical study [6]. The experimental source was supplied by the national meteorological data catalogue [7] where a mean climatic day is defined for each month of the year. Between other quantities, the average daily total of the direct solar radiation G (Wh/m^2) on horizontal surface and the hourly distributions of T_a and of d are given for every month of the idealised mean meteorological year. These hourly variations have been obtained by averaging the measures of T_a and of d recorded in Pisa airport at the same hour of every day of the given month over a great number of years.

The mathematical description of the inclination of the sun rays at any hour of the year completed the desired assessment of the time and space variation of T_i^* and thus of T_a^*, all over the boundary surfaces of the Tower.

Fig. 2 illustrates, as example, the polar diagrams of i acting on the basement and the shaft at different hours of respectively the mean summer and winter solstice days (21st June, 21st December).

3 Transient thermal analysis

3.1 Simulation tools and meshing

The overall numerical simulation of the interaction between the Tower and the climatic agents has been performed with program ANSYS, versions 5.1 and 5.2. Three different computers have been used contemporary in order to let output checks and post processing operations be executed by means of other appositely created programs at the same time that a new simulation was running.

Particular attention has been paid for the mesh construction of the cross sections of the basement, of the shaft and of the single columns. Since the three investigated problems have been reduced to 2D, the ANSYS library element PLANE55 has been selected for all the simulations. This element is the easier and faster library element for heat conduction and convection analysis and has confirmed its reliability in precedent studies [4].

The mesh was given a polar symmetry in order to almost get constant topological properties for any azimuth direction since it happens that every part of

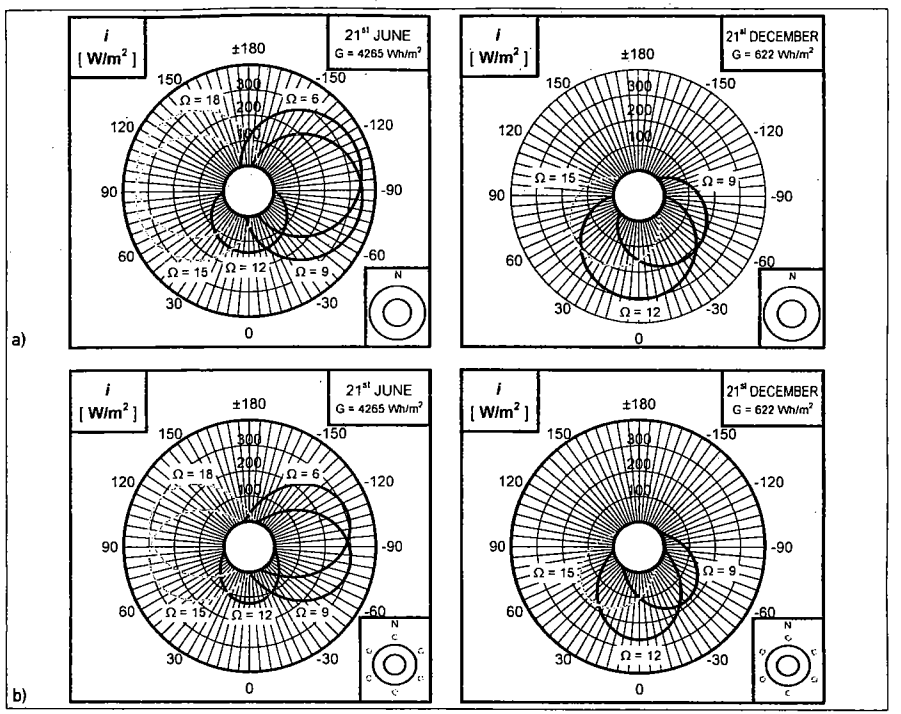

Fig. 2. Hourly distribution of the normal component of the direct solar radiation acting, a) on the basement surface and b) on the shaft surface during the mean 21st of June and during the mean 21st of December
Bild 2. Stündliche Verteilung der Normalenkomponente der direkten Sonneneinstrahlung auf, a) die Fundamentoberfläche, b) die Schaftoberfläche im Verlaufe eines 21. Juni und eines 21. Dezembers

the outer surface is submitted, in some time of the year, to direct solar radiation and therefore any radial direction had to intersect circa the same number of nodes and elements.

Furthermore the mesh was also requested to have a greater nodal density and a better element definition near the external surfaces where the heat exchanges with the environment take place and the temperature distributions were expected to be more complex. On the other hand we were allowed to decrease the number of nodes and elements in the internal part of the Tower, since the temperature distributions were foreseen to be here more uniform. By doing that we reached the same output simulation accuracy with a minimal calculation-time consumption and focused our attention on the parts where a finer information degree was requested. Following these criteria the meshes in Fig. 3 have been developed respectively for the basement, the shaft, and the columns.

The meshes of both these two models are composed by 240 nodes and 240 elements, meanwhile the mesh of the column is composed by 49 nodes and 40 elements.

3.2 Time stepping

The transient simulation was subdivided into several time steps, each of them characterised by a specific input set related to a particular instant of the simulated mean meteorological year.

With simulated time we mean the number of seconds within a simulated time interval (hour, day, month) while the calculation time is the number of real seconds required by the computer to perform the calculation of the thermal interaction Tower-environment in the simulated time interval. To give an idea, to simulate a whole climatic year almost 3 days of calculation time are needed.

In order to get good transient results it is essential to have a fine and smooth input versus simulation time. For this reason, the minimal time-step has been set to 5 minutes of simulation time.

That means that every simulated day is composed by 288 time steps and that every simulated year contains 105120 time steps each of them with completely different inputs features since the values of air temperature values and intensity and direction of the sun radiation change, as previously seen, from instant to instant.

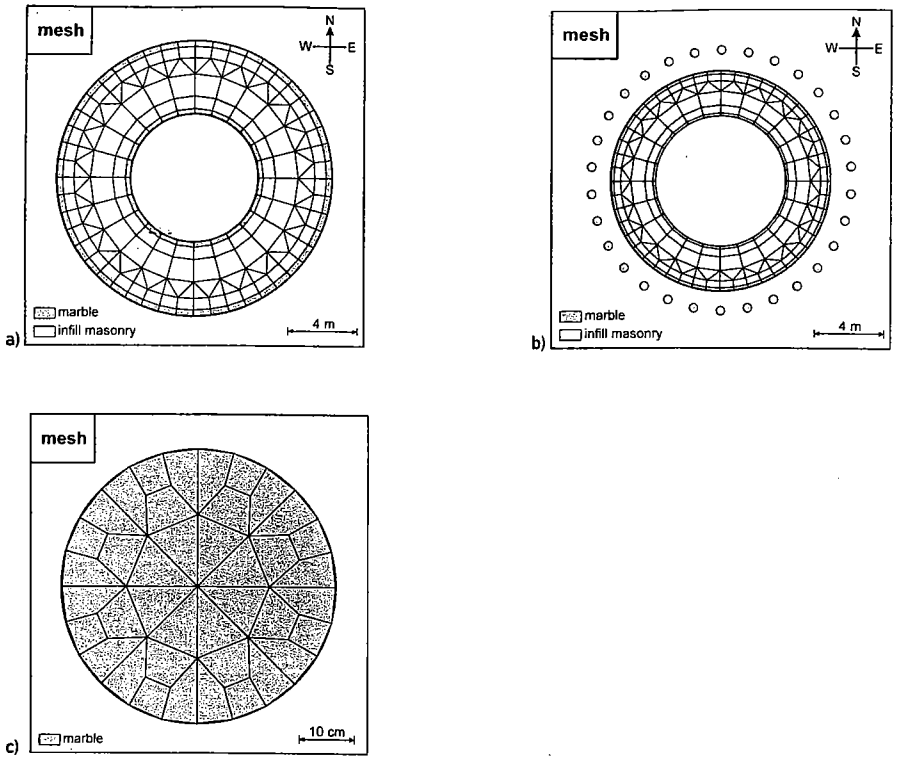

Fig. 3. Meshes, a) of the idealized basement cross section, b) of the idealized shaft cross section, c) of a typical column cross section
Bild 3. Diskretisierung, a) des idealisierten Fundamentquerschnitts, b) des idealisierten Schaftquerschnitts, c) eines typischen Säulenquerschnitts

4 Temperature fields

Hereafter are reported some significant temperature fields resulted from the numerical simulation.

Between all the 365 days of the mean meteorological year during which the hourly evolutions of the thermal fields have been calculated, the two summer and winter solstice days, i. e. the days of the year with respectively the longer and the shorter period of solar radiation, have been selected as time windows to give a meaningful idea of the complexity of this physical phenomenon both in summer and in winter conditions.

The principal results, i. e. the daily temperature extremes, together with their happening instants and locations are collected in Table 2.

4.1 Basement

a) summer conditions

The temperature distributions calculated over the idealised cross section of the basement at different hours of the mean 21st June are reproduced in Fig. 4.

Intense radial temperature gradients rise up locally at the external boundary zones under the influence of the direct solar radiation but they quickly attenuate with the depth and are almost absent in the central part of the infill masonry.

It can be seen from Fig. 2 that in summer the greater amounts of radiation energy are transferred to the Tower at the east side during the morning and at the west side during the afternoon because at these times the inclination of the sun rays is lower and, even if the intensity of the radiation is not yet maximum, the energy adsorption is greater than at noon.

For this reason the local radial gradients and the surface temperatures, at the east side in the morning, and at the west side in afternoon, are greater than those at the south side at noon. Moreover, it can be observed that they reach their daily absolute maximum at the west side in the afternoon in spite that the time distribution of the radiation is symmetrical with respect to midday since the Tower leans almost perfectly southwards.

Table 2. Extremes punctual temperatures in the basement and in the shaft during the mean 21st June and the mean 21st December
Tabelle 2. Extremwerte der Temperatur im Fundament und im Schaft am 21. Juni und 21. Dezember

	BASEMENT							
	summer conditions (21st June)				winter conditions (21st December)			
	T (°C)	Hour	I/F	O	T (°C)	Hour	I/F	O
Minimum	16.9	0.00	I	N	6.9	8.00	F	N
Maximum	33.9	18.00	F	W	16.7	15.00	F	S
	SHAFT							
Minimum	16.6	4.00	F	S	6.6	8.00	F	N
Maximum	31.8	18.00	F	W	14.8	17.00	F	S-W

(E = east, F = facing, I = infill, N = north, O = orientation, S = south, W = west)

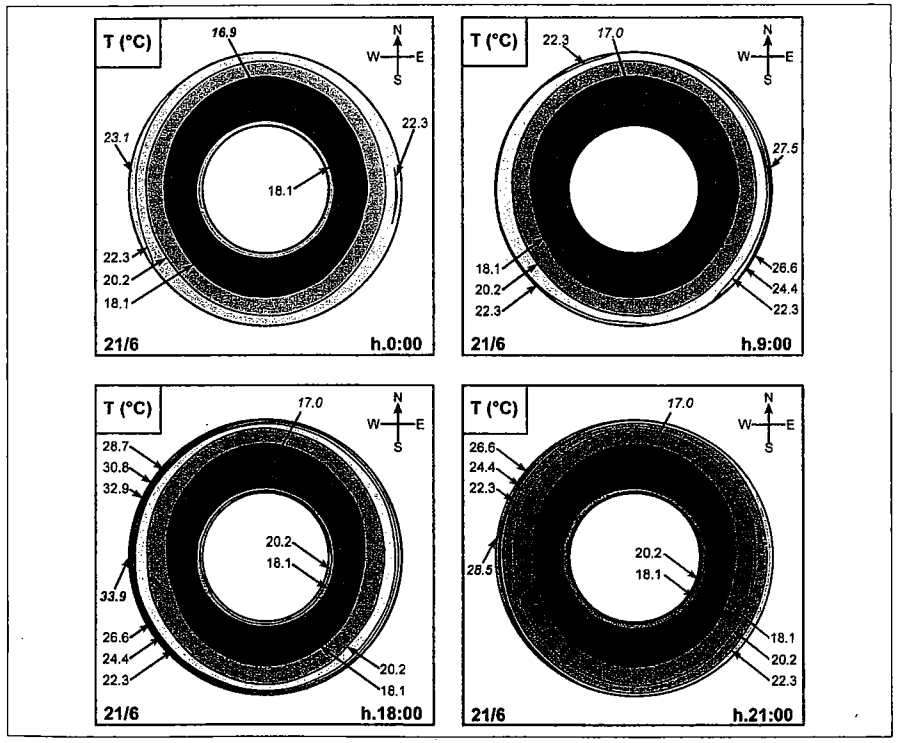

Fig. 4a. Time evolution of the temperature fields over the idealized cross section of the basement during the mean 21st June day
Bild 4a. Zeitabhängige Entwicklung des Temperaturfeldes über den Fundamentquerschnitt am 21. Juni

The reason of this time asymmetry of the thermal behaviour of the monument is that the mean temperature of the Tower is greater in the afternoon due to the accumulation process of adsorbed solar energy along the day.

At the end of its time interval of direct irradiation, a generic piece of surface gets shadowed and cools down while the temperature wave slowly propagates from the surface towards the centre contemporary attenuating its intensity.

This interesting aspect is well evidenced at t = 0.00 h by the little spot in the infill masonry near the east side, where the temperature (T = 22.3 °C) is greater than in the neighbourhood. This warm spot represents what remains of the thermal impulse produced by the direct radiation at the surface in the precedent morning.

b) winter conditions

Let us compare the temperature fields calculated in winter with those calculated in summer conditions.

Leaving apart the obvious remark that winter temperatures are generally lower than summer temperatures, the dominant aspects of the thermal behaviour of the basement are in winter very different than in summer.

The only common aspect is that extreme local gradients always occur at the boundaries as a logical consequence of the surface heat exchanges strongly variable with time.

But when in winter the peripheral zones are, during the night, colder than the inner parts and the minimum temperature (T = 6.9 °C) is reached at t = 8.00, in summer on the contrary night minimum temperatures (T = 16.9 °C) take place at t = 0.00 in the infill masonry while the boundary zones remain relatively warm.

Under the effect of the direct radiation during a cloudless winter day a temperature wave builds up at the southern external surface reaching the maximum (T = 16.7 °C) at t = 15.00 and propagates later mainly in the south-north direction with a contemporary intensity attenuation.

This result well agrees with the daily distribution of the direct solar radiation on the outer surface of the basement since it can be seen from Fig. 2 that in winter the incoming solar energy attains its greater value exactly at noon on the southern side.

In summer something similar happens but essentially in the east-west direction at morning and in the west-east direction in the afternoon, as already seen.

Moreover, the temperature fields are in winter relatively more symmetrical with respect to the south-north axis than in summer, due to the prevalence of the southern irradiation and to the minor importance of global warming.

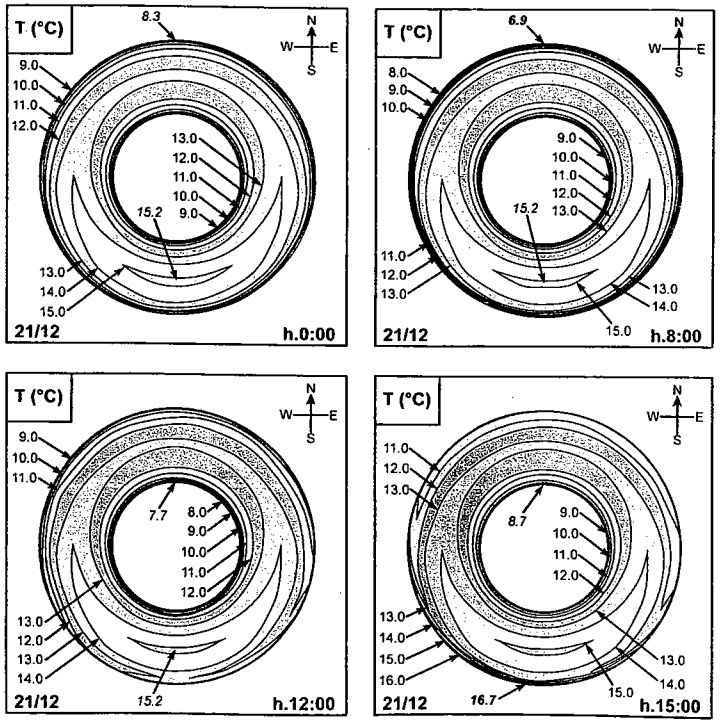

Fig. 4b. Time evolution of the temperature fields over the idealized cross section of the basement during the mean 21st December day
Bild 4b. Zeitabhängige Entwicklung des Temperaturfeldes über den Fundamentquerschnitt am 21. Dezember

4.2 Shaft

a) summer conditions

The temperature distributions calculated over the idealised cross section of the shaft at different hours of the average 21st June day are reproduced in Fig. 5a.

Comparing the summer thermal behaviour of the shaft with that of the basement, the same relevant features that have already been pointed out for the basement, can be qualitatively recognised also in the shaft with the difference that here the local radial gradients are smaller than in the basement because of the shielding offered by the columns and the lodges against the direct solar radiation.

The biggest difference attains the daily minimum temperature which is reached, as already said, in the shaft at the external south surface at t = 4.00 h while in the basement it was reached in the northern part of the infill masonry at t = 0.00 h.

This result can be explained with the fact that the northern external surface of the shaft is direct irradiated at the sunrise and at the sunset while, on the contrary, the southern surface remains always shadowed by the lodges since on the 21st June the sun rays reach at noon their greatest inclination and are almost vertical.

b) winter conditions

The temperature distributions calculated over the idealised cross section of the shaft at some hours of the average 21st December day are reproduced in Fig. 5b.

The thermal behaviour of the shaft during this day is qualitative analogous to that of the basement since the temperature fields have a similar shape and the daily minimum temperatures are in both cases

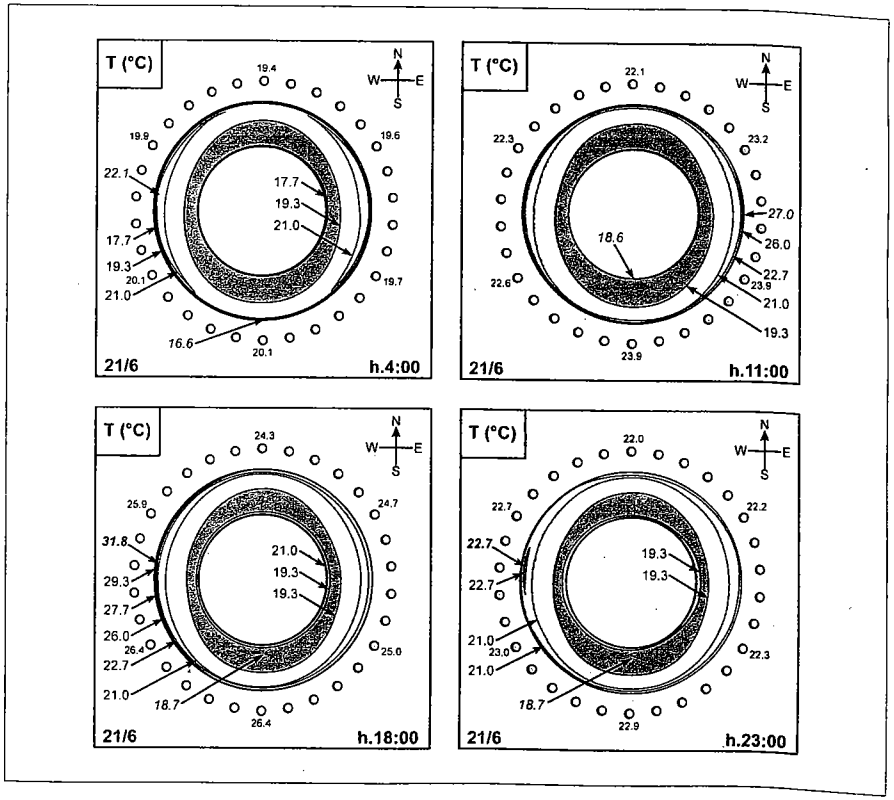

Fig. 5a. Time evolution of the temperature fields over the idealized cross section of the shaft during the mean 21st June day
Bild 5a. Zeitabhängige Entwicklung des Temperaturfeldes über den Schaftquerschnitt am 21. Juni

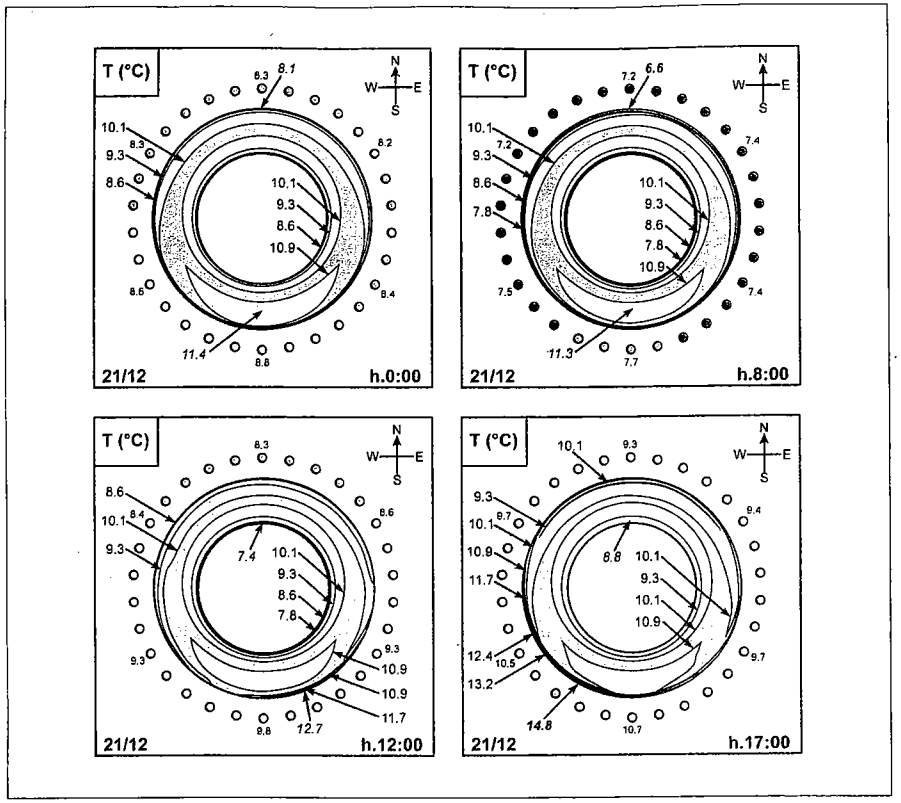

Fig. 5b. Time evolution of the temperature fields over the idealized cross section of the shaft during the mean 21st December day
Bild 5b. Zeitabhängige Entwicklung des Temperaturfeldes über den Schaftquerschnitt am 21. Dezember

reached at the same hour and have almost the same value.

The main difference attains the daily maximum temperature which in the basement takes place at t = 15.00 h at south (T = 16.7 °C) while in the shaft, due to the shadowing effects of the lodges and of the columns, it is reached some later at t = 17.00, in a more western position and has a lower value (T = 14.8 °C).

4.3 Columns

The thermal behaviour of the columns differs very much from those of the basement and of the shaft essentially because of their much lower thermal inertia and also because of the very different direct solar radiation conditions.

The calculation of the temperature fields in the columns has been performed with the main aim to calculate the time distribution of their Effective Mean Temperature (see § 5.2) which is responsible of length variations. It can be argued indeed that the length variations of the columns with respect to the shaft must be the main source of thermal movements and eigenstresses in the Tower while on the contrary, end rotations due to the effect of the Effective Linear Gradients within the diameter of each column are, under this aspect, negligible.

Fig. 6 relate to the most southern column (column No. 1) and respectively show two temperature fields calculated for the average 21st June and two temperature fields calculated for the average 21st December. Each field contains the daily maximum or the daily minimum punctual temperatures. It can be observed how the isothermal lines are almost concentric during the night both in summer and in winter meaning that almost no night Effective Linear Gradient takes place.

As for the basement, the highest temperatures and the greatest gradients are reached in this column at west in summer (t = 17.00) and at south-southwest in winter (t = 15.00) but maximum temperatures are in the column always greater than the corresponding

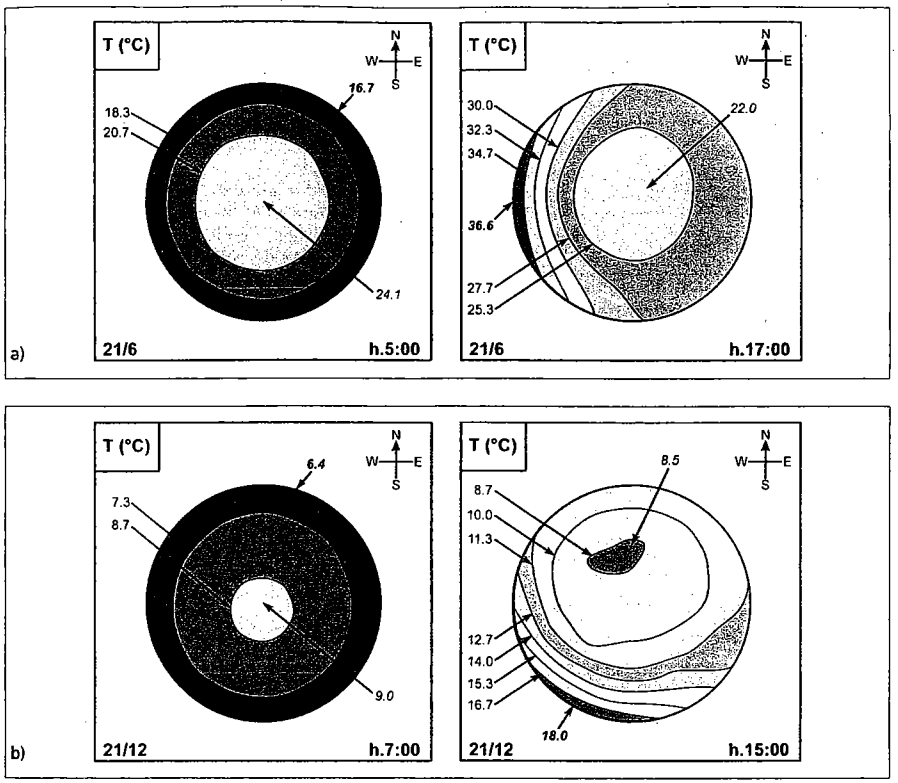

Fig. 6. Time evolution of the temperature fields over the cross section of the southernmost column (column No. 1), a) during the mean 21st June day, b) during the mean 21st December day
Bild 6. Zeitabhängige Entwicklung des Temperaturfeldes über den Querschnitt der südlichsten Säule (Nr. 1), a) am 21. Juni, b) am 21. Dezember

basement temperatures (about 3 °C in summer and 1 °C in winter).

Fig. 7 shows the hourly distribution of the temperature along the mean 21st day of June in five points of the meridian diameter of the cross section. To be noticed the damping of the temperature oscillations of the inner points. Thermal analyses in summer and winter conditions have been performed for columns No. 1, 6, 11, 16, 21, 26 equally spaced all around the Tower (for the location of the columns see Fig. 8).

5 Effectfive mean temperatures and effective global linear gradients

In order to better understand the overall thermal behaviour of the Tower it is useful to synthetize the enormous amount of informations into few significant quantities like the Equivalent Mean Temperature and the Effective Global Linear Gradients as indicated hereafter.

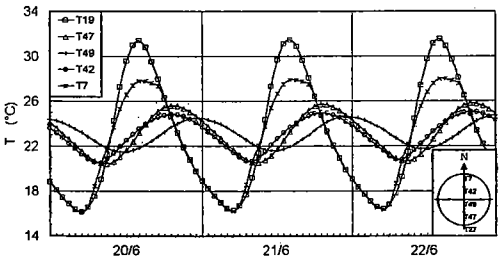

Fig. 7. Daily evolution of the temperature calculated in five points of the meridian diameter across the southernmost column (column No. 1) during the mean 21st June day
Bild 7. Entwicklung der Temperatur über den Tag, berechnet in 5 Punkten auf der Durchmesserlinie der südlichsten Säule Nr. 1 am 21. Juni

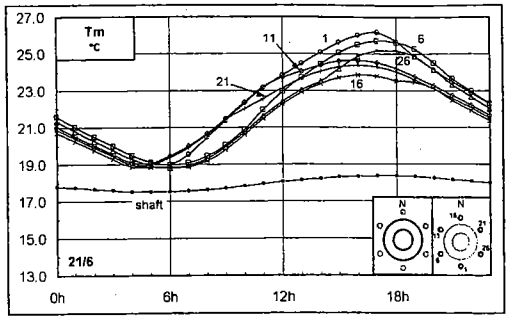

a)

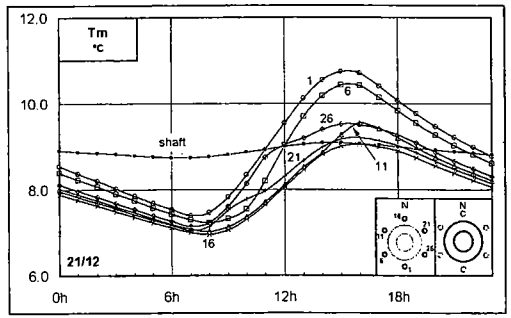

b)

Fig. 8. Hourly distributions of the E.M.T. of columns 1, 6, 11, 16, 21, 26 and of the shaft calculated, a) during the mean 21st June, b) during the mean 21st December
Bild 8. Entwicklung der E.T.M. der Säulen 1, 6, 11, 16, 21, 26 und des Schafts berechnet im Stundentakt, a) am 21. Juni, b) am 21. Dezember

5.1 Basic assumptions

We have already supposed negligible the variation of the thermal fields along the axial direction of the Tower. Moreover, if we assume as infinitely rigid the annular masonry structures that at each order bear, together with the columns, the round walks of the lodges (see Fig. 1), any cross section of the Tower remains plane.

It is known that if such conditions apply, it can be demonstrated by means of the strain suppression method [8] that any instantaneous, nonlinear, 2D temperature field may be decomposed into:

a) A uniform part T_m, [°C], which is responsible of the axial displacements of the cross section centroid and is therefore called Effective Mean Temperature (E.M.T.).

b) Two temperature distributions linearly variable along the x and the y centroidal principal axes of the sections, defined by their gradients DT_x, DT_y [°C/m] which are responsible of the rotations of the sections around respectively the y and the x axes and are therefore called Effective Global Linear Gradients (E.G.L.G.). Here, due to the polar symmetry of the idealised cross sections, any radial direction is a principal one. Therefore the x axis has been taken coincident with the W-E direction and the y axis with the S-N direction.

c) A residual, non-linear, self-compensated part B (x, y) which is responsible of the primary eigenstresses [5].

In the present case the E.M.T. is given by relation (8).

The E.G.L.G. along the x axis is given by relation (9) and is assumed positive if the east side is warmer than the west side.

The E.G.L.G. along the y axis is given similarly by relation (10) and is assumed positive if the north side is warmer than the south side.

In the preceding relations index 1 denotes S. Giuliano marble and index 2 denotes infill masonry. Simple apex ' is related to the inner marble facing while double apex " regards the outer marble facing. Therefore:

$$J'_{x1},\ J''_{x1},\ J_{x2} \qquad J'_{y1},\ J''_{y1},\ J_{y2}$$

are respectively the moments of inertia of the inner marble facing, of the outer marble facing and of the infill masonry with respect to the x and to the y axis, while

$$A'_1,\ A''_1,\ A_2$$

are respectively the areas of the same corresponding parts. A_c is the area of the cross section of one column, $n_E = E_1/E_2$ is the mechanical homogenization coefficient (ratio between the *Young*'s Modulus of the marble (E_1) and that of the infill masonry (E_2)), $n_\alpha = \alpha_1/\alpha_2$ is the thermal homogenization coefficient (ratio between the thermal linear expansion coefficient of the marble (α_1) and of the infill masonry (α_2)), N = 30 is the number of the columns at each order.

It must be noticed that the *Young*'s Modulus of the S. Giuliano marble is quite a well defined quantity due to the great homogeneity and the excellent mechanical properties of this material (see Table 1).

The determination of an average bulk *Young*'s Modulus of the infill masonry is on the contrary rather uncertain since this part of the Tower presents very scattered mechanical properties and is also characterized by a diffuse presence of voids and of stones of different sizes randomly distributed within its mass.

Based on the compression test results of cylindrical masonry champions of the Tower [3] it can be seen that n_E is variable between 6 and 4. In the present study the conservative value $n_E = 4$ has been assumed.

The determination of n_α is even more uncertain since no direct measurements of α_1 and α_2 have been performed. Here the value of $n_\alpha = 0.5$ has been taken according to common literature data on similar materials.

The radial direction along which the resultant Effective Linear Gradient is maximum is given by

$$\operatorname{tg}\varphi = \frac{DT_y}{DT_x} \tag{11}$$

where the angle φ is measured with respect to the x axis.

The intensity of the maximum Effective Linear Gradient is of course

$$DT_{max} = \sqrt{DT_x^2 + DT_y^2}. \tag{12}$$

To manage the large amount of output data and proceed in the analysis, three macros in ANSYS language has been programmed so that it was possible to calculate, for every part of the Tower and at each instant, the E.M.T. and the E.G.L.G. along the x and y axes.

5.2 Effective Mean Temperature

The E.M.T. oscillations have a little amplitude in the basement and therefore they are not reported here. Remarkable E.M.T. differences result on the contrary between shaft and columns. Fig. 8 evidence the time dependence of the E.M.T. in the six sample columns and in the shaft from the apparent daily course of the sun in summer and in winter conditions.

The calculated E.M.T. hourly distributions are in agreement with the qualitative expectations that could be logically drawn taking into account the effects of mutual shadowing of the columns.

Regrettably no comparison with experimental results is possible since until now no temperature measurement have yet been performed in the columns.

To be noticed that the southernmost column (column No. 1) experiences in summer a daily E.M.T. oscillation of about 7.5 °C while the maximum E.M.T. difference takes place between the southernmost and the northernmost column (column No. 16) at t = 16.00 and is of about 2.5 °C.

Moreover, all the columns have in summer a higher E.M.T. than the shaft and therefore they are always submitted to daily oscillating compressive efforts in addition to gravitational compressive stresses.

In winter, on the contrary, the E.M.T. of almost all the columns is lower than that of the shaft with the exception of only columns No. 1 and No. 6 whose E.M.T. significantly exceeds that of the shaft during some hours in the afternoon. It can thus be argued that all these columns are expected to be submitted in winter to daily decompression cycles due to thermal effects.

5.3 Effective Global Linear Gradient

Fig. 9 and 10 contain the diagrams of the daily variation of the E.G.L.G., whose components are at any instant DT_x and DT_y.

In the diagrams, the origin coincides with the centre of the Tower, the horizontal axis with the x axis (W-E direction), the vertical axis with the y axis (S-N direction).

5.3.1 Basement-Daily evolution of the resultant E.G.L.G.

The diagrams of Fig. 9 evidence that a diurnal phase is clearly distinguishable from a night phase. During the morning DT_x exhibits positive values until a maximum is reached near 10.00 h. DT_x than progressively diminishes, changes its sign between 14.00 and 15.00 h (near 13.00 h in December) and reaches a minimum at the sunset.

During the night the global cooling down of the basement produces in summer and in winter a progressive, slow migration of DT_x towards zero which is interrupted by the next sunset.

At any day of the year DT_y is always negative, that is, the south side is always warmer than the north side. But while the hourly evolutions of DT_y in winter (December), spring (March) and autumn (September) are each other qualitative similar and are characterised by large daily oscillations, near the summer solstice DT_y approaches zero and its daily oscillations are little compared with those of DT_x.

$$T_m = \frac{n_E n_\alpha \left[\iint_{A'_1} T(x,y)\,dA'_1 + \iint_{A''_1} T(x,y)\,dA''_1 + A_c \sum_{i=1}^{N} T_i(x_i, y_i) \right] + \iint_{A_2} T(x,y)\,dA_2}{(A'_1 + A''_1 + N \cdot A_c)\, n_E + A_2} \tag{8}$$

$$DT_x = \frac{n_E n_\alpha \left[\iint_{A'_1} T(x,y)\,x\,dA'_1 + \iint_{A''_1} T(x,y)\,x\,dA''_1 + A_c \sum_{i=1}^{N} T_i(x_i, y_i)\,x_i \right] + \iint_{A_2} T(x,y)\,x\,dA_2}{\left(J'_{y1} + J''_{y1} + A_c \sum_{i=1}^{N} T_i(x_i, y_i)\,x_i^2 \right) n_E + J_{y2}} \tag{9}$$

$$DT_y = \frac{n_E n_\alpha \left[\iint_{A'_1} T(x,y)\,y\,dA'_1 + \iint_{A''_1} T(x,y)\,y\,dA''_1 + A_c \sum_{i=1}^{N} T_i(x_i, y_i)\,y_i \right] + \iint_{A_2} T(x,y)\,y\,dA_2}{\left(J'_{x1} + J''_{x1} + A_c \sum_{i=1}^{N} T_i(x_i, y_i)\,y_i^2 \right) n_E + J_{x2}} \tag{10}$$

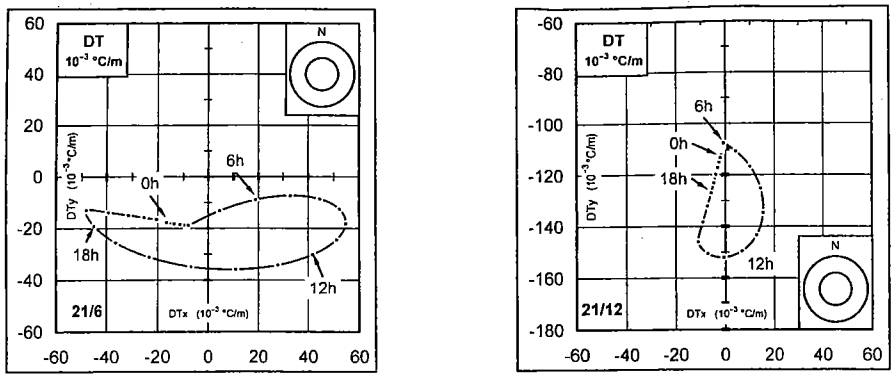

Fig. 9. Daily evolution of the resultant E.G.L.G. of the idealized cross section of the basement calculated, a) during the mean 21st June day, b) during the mean 21st December day
Bild 9. Entwicklung der resultierenden E.G.L.G. des Fundamentquerschnitts berechnet über den Tag, a) am 21. Juni, b) am 21. Dezember

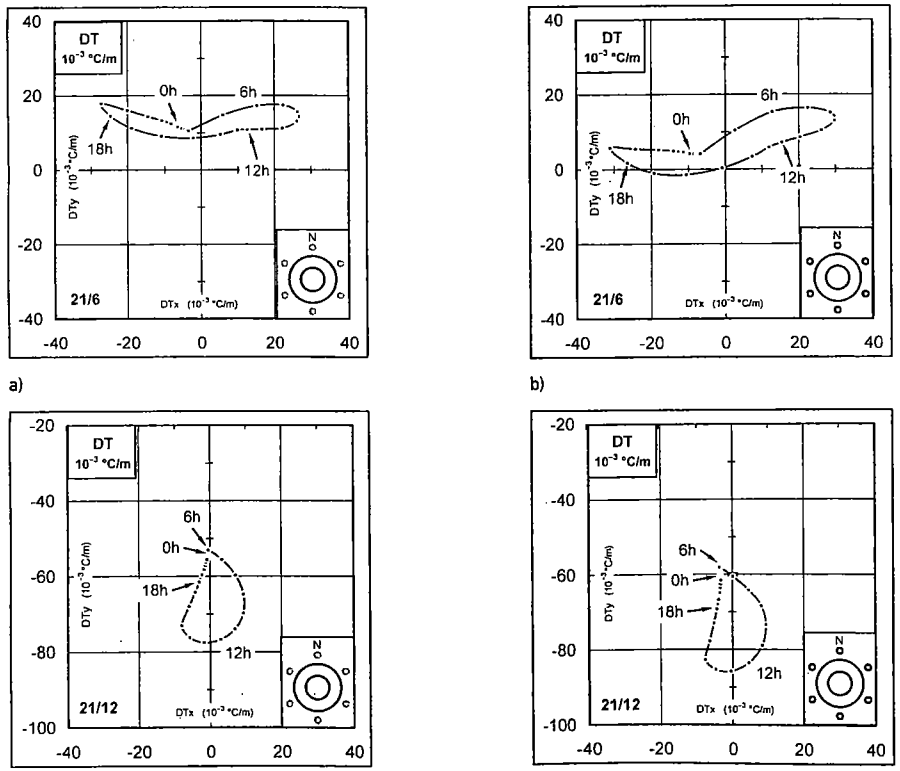

*Fig. 10. Daily evolution of the E.G.L.G. of the idealized cross section of the shaft calculated **without**, a) and **with**, b) the contribution of the columns during the mean 21st June day and during the mean 21st December day*
*Bild 10. Entwicklung der E.G.L.G. des Schaftquerschnitts **ohne**, a) und **mit**, b) Einfluß der Säulen, berechnet über den Tag am 21. Juni und am 21. Dezember*

To understand this result it must be noticed that during the morning of the mean June day the sun shines almost horizontally over the north-east side of the basement and, although the radiation intensity is still rather low, the amount of adsorbed energy is considerable since the sun rays are almost perpendicular to the external surface. That is why DT_y, still remaining negative, tends in the early hours to positive values (north side warmer than south side). The same thing happens at the north-west side in the afternoon.

5.3.2 Shaft-Daily evolution of the resultant E.G.L.G.

Looking in Fig. 10 at the corresponding E.G.L.G. diagrams of the shaft, we find that they qualitatively maintain the same peculiarities of those of the basement with the exception of DT_y which reaches positive values in June (north side warmer than south side) under the effect of the direct solar radiation at the beginning and at the end of the day. The shadowing effects produced by the columns and the lodges are clearly recognizable in the attenuation of E.G.L.G. magnitudes, particularly around the noon hours.

If we take into account the E.M.T. of the columns when calculating E.G.L.G. according to relations (9) and (10), we obtain a significant magnification contribute both of DT_x and DT_y, as can be seen from Fig. 10, thus confirming the important role played by the columns in the thermal response of the Tower.

6 Conclusions

The theoretical model here proposed, although conceptually very simple, revealed able to provide almost a complete picture of the dominant aspects of the complex time and space variable temperature fields induced in the Leaning Tower by the climate.

The enlargement of the actually available database of in situ measurements (temperatures, solar radiation, thermal properties of the materials) would allow the optimization of the prediction performances of the model by retrofitting or substituting some here hypothesized physical parameters.

The evidenced important role played by the columns in the overall thermal behaviour of the Tower suggests moreover to extend the temperature monitoring to a sufficient number of them.

The calculated daily distributions of synthesis quantities like the Effective Mean Temperature and the Effective Global Linear Gradient constitute the basis for simple estimation of the thermal movements and eigenstresses of the Tower for strengthening or restoring purposes.

References

[1] Ministero dei Lavori Pubblici: "Ricerche e Studi su la Torre Pendente di Pisa e i fenomeni connessi alle condizioni d'ambiente", Commissione per il Consolidamento della Torre pendente di Pisa (legge 19 maggio 1965, no. 506). Istituto Geografico Militare, Firenze, 1971.

[2] *Camuffo, D.*: "Torre di Pisa – Studio di analisi del microclima e delle interazioni ambiente-manufatto", Rapporto interno del Comitato Internazionale per la Salvaguardia della Torre, 1995.

[3] ISMES: "Torre di Pisa – Determinazione di caratteristiche fisiche e di resistenza meccanica di campioni prelevati dalle murature della Torre", Prog. DGM/4136.A, Doc.REL/DGM/00135, 1987.

[4] *Froli, M., Hariga, N., Nati, G., Orlandini, M.*: "Longitudinal Thermal Behaviour of a Concrete Box Girder Bridge", Structural Engineering International, no. 4 (1996), pgg. 237–242.

[5] Comite Euro International du Beton: "Thermal Effects in Concrete Structures" , Report No. 167, 1985.

[6] *Froli, M., Ulivieri, E.*: "Sull'irraggiamento solare della Torre Pendente di Pisa", Rapporti di Studi e Ricerche del Dipartimento di Ingegneria Strutturale dell'Università di Pisa, No. 5, 1998.

[7] Consiglio Nazionale delle Ricerche: "Dati climatici per la progettazione edile ed impiantistica", Roma, 1982.

[8] *Froli, M., Ulivieri, E.*: "Transient Temperature Fields induced by the Climate in the Leaning Tower of Pisa", Rapporti di Studi e Ricerche del Dipartimento di Ingegneria Strutturale dell'Università di Pisa, No. 7, 2000.

Authors of this paper:
Prof. Ing. Maurizio Froli, Dipartimento di Ingegneria Strutturale dell'Università di Pisa, Via Diotisalvi 2, I-56126 Pisa
Dr.-Ing. Enrico Ulivieri, Siemens AG – ZT MS 2, Otto-Hahn-Ring 6, D-81730 München

Maurizio Froli
Paolo Formichi

Statistical analysis of temperature measurements in the Leaning Tower of Pisa in comparison with theoretical predictions

The wide amount of temperature measurements collected in the shaft of the Leaning Tower of Pisa during four years monitoring is here analysed by means of statistical methods and compared with the theoretical values calculated with a FEM analysis in a precedent work, where the transient boundary conditions reproduce the hourly variations of the main meteorological agents all over an idealised, mean meteorological year.

Statistische Auswertung der Temperaturmessungen am Schiefen Turm von Pisa im Vergleich mit den theoretischen Vorhersagen. Die große Anzahl der Temperaturmessungen, die über einen Zeitraum von vier Jahren am Schiefen Turm von Pisa vorgenommen wurden, werden unter Verwendung statistischer Methoden ausgewertet und mit den Ergebnissen der theoretischen Berechnungen mittels FEM verglichen. Hierbei werden die instationären Randbedingungen, die die stündlichen Veränderungen der wesentlichen meteorologischen Einflüsse hervorrufen, als idealisiertes meteorologisches Jahr erfaßt.

1 Introduction

The movements of the Tower, even when very small, have of course always been a great concern source for those who were charged to look after its stability and maintenance all along the centuries of its life.

In 1934, with the employment of high precision instruments like the *Girometti-Bonechi* level which allowed slope variation measurements with the sensibility of ±0".01, it was clearly evidenced the existence of doubly cyclical movements due to the daily and yearly evolution of the sun radiation and of the other climatic agents which developed in superimposition to the general slope increase produced by the well known soil settlements [1]. At the same time it was found out that daily slope variations of climatic origin had the same amplitude of the yearly out of plumb increase (~5") which progressed every year for geotechnical reasons before stabilisation measures were applied in the years between 1991 and 2000. Since 1934, attention was than also paid to the thermal behaviour of the Tower in the attempt to achieve a better general understanding of this complex phenomenon which could not be ignored in the measuring operations of the progressive inclination.

With the time it became also clear that a deeper knowledge of the thermal response of the monument could have helped to enlighten some not still completely cleared facts like the circumferential cracking of the lodge vaults occurring prevalently at the southern side and the periodical breaking up of some columns, as well as the reason why the foundation rotates cyclically [2]. Theoretical studies of the microclimate in the immediate neighbourhood of the Tower were indeed performed for limited time periods and also temperature measurements were taken on some portion of its outer surface [3].

Being but limited to the boundary surfaces, these investigations cannot give a realistic and complete picture of the temperature fields acting within the very thick walls of the monument if not integrated with a adequate theoretical modelling of the inner heat fluxes. This work has been performed in [4], where the boundary conditions have been more simply deduced from literature average climatic data. In the present paper a comparison is stated between temperature fields calculated by that way and statistically analysed, in situ temperature measurements.

2 Temperature measurements in the Leaning Tower

Since 1934 the inner air temperature of the ground floor chamber was recorded by means of a thermometer.

In 1966 temperature measurements started to be regularly taken within the walls of the Tower by means of ten thermocouples inserted in some holes previously drilled in the masonry at different places in order to extract cylindrical stone specimens. Two other air thermometers were also installed outdoor at the top of the Tower and indoor at the ground level; the measurement operations began on July 1967.

In 1989 thermocouples were substituted with electronic sensors and the experimental temperature data started to be regularly transmitted every hour, by means of VHF, to a special operative section of the local Public Works Office, printed on paper and stored on magnetic tapes by means of computer facilities.

In 1991 the International Committee of experts (Comitato Internazionale per la Salvaguardia della Torre di Pisa) co-ordinated by Prof. *Jamiolkowski* decided that the whole monitoring equipment of the Tower necessitated to be expanded and updated including also the existing facilities for measuring, transmitting and recording temperature data.

Five electronic sensors (N° 67, 68, 69, 70, 71) were installed in the northern hole and five (N° 103, 104, 105, 106, 107) in the southern hole (see Fig. 1).

Two additional sensors measured shade air temperature at the top of the Tower and indoor temperature at the ground level chamber. A solarimeter and a anemoscope were also installed at the top of the belfry.

Every hour each sensor executes a temperature measurement which is then electronically stored on magnetic support, compatible with current PC software.

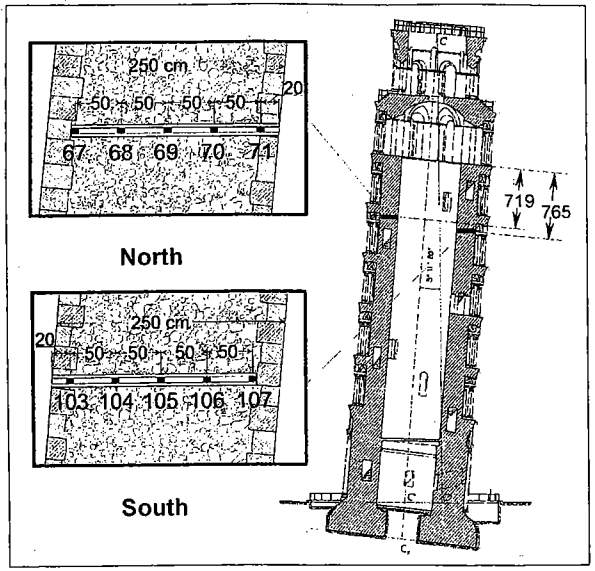

Fig. 1. Location of the electronic sensors for the temperature measurement within the walls of the Tower
Bild 1. Anordnung der elektronischen Sensoren für die Temperaturmessung innerhalb der Turmwände

The data set used in the present study is made up, for each of the ten sensors, by approximately 35000 hourly temperature records collected during the period 1996–1999. Due to some malfunctioning of the recording devices unfortunately temperatures were not registered during seven months in 1997 and three months in 1999.

Temperature measures still continue to be performed with the same facilities and the same temporal resolution and shall be used in future to enlarge the extension of the data base and to improve the refinement degree of the statistical analyses.

3 Statistical analysis of temperature data

3.1 Hypotheses

In a precedent paper [4] the thermal response of the Tower was theoretically analysed by means of a FEM 2D model, where the transient heat flux boundary conditions had been built up under the assumption that climatic conditions reproduce every year exactly those of the mean meteorological year. This idealised year is described in [5] and is based on the measurement of the main climatic agents (wind velocity, shade air temperature, direct and diffuse solar radiation) repeated for many years in the nearest meteorological station (Pisa airport) at each hour of every day of the year. Each month of the mean meteorological year is characterised by a mean monthly meteorological day where any single hourly value of a given climatic agent is obtained by averaging all the available measurements performed at that hour all the days belonging to all the homonymous months.

In order to institute a homogeneous comparison between the theoretical predictions thus obtained and the measurements performed in the Tower, also the statistical analysis had to be developed under the simplifying hypothesis of climatic steady periodicity, meaning that the weather is assumed to remain approximately steady during each month and to repeat unchanged every year. From a statistical point of view, this procedure was also necessary in order to get random samples with a significant number of elements in spite the relatively few monitoring years. In the future, when a larger number of temperature measurements shall be available, it will be possible to build up sufficiently large random samples even on more restricted time windows, thus increasing the accuracy of the statistical analysis.

Finally, for sake of homogeneity and of simplicity too, each temperature value has been entirely considered a random event, thus ignoring the possibility to partially give the daily and the yearly periodic oscillations a deterministic meaning following the obvious remarks that surely outdoor air temperatures are at night lower than during the day and that winter is colder than summer [6].

3.2 PDF identification of the random samples

Following these principles, twenty-four random samples of temperature measures have been built up for each of the ten sensors and each of the twelve months of the year.

Each sample contains all the available temperature measurements collected during the recording period at the same hour every day of all the corresponding months.

Altogether 2880 random samples of the size of about 90 elements each have been gathered.

The choice of the Probability Density Function (PDF) that could best fit the distributions of all the random samples was necessary as a preliminary step in the statistical analysis. In order to reduce the calculation time, just a certain number of significant random samples have been selected for PDF identification. The space locations are those of sensors N° 67, 69, 71 on the northern side and sensors N° 103, 105, 107 on the southern side, corresponding in both cases to the peripheral and the middle measuring spots within the thickness of the walls (Fig. 1); the chosen months are March, June, September and December (solstice and equinox months) and since solar radiation is the most important dispersion source in the thermal response of structures, the measuring instant has been fixed at 12.00 a.m. where global solar radiation on horizontal surface always attains its daily maximum in cloudless days.

The Normal Probability Function (*Gaussian*), the Log-Normal Probability Function and the *Gumbel* Probability Function (Type I) have been used for best fit checks by plotting the random samples on the corresponding probability papers for thoroughly 72 diagrams.

Fig. 2 and 3 collect here for example only the results related to sensor 67 (next to the outer surface) and 105 (at middle thickness) in the month of June while the complete set of diagrams can be found in [7]. Each figure regards a given monthly random sample and contains the three tested distributions whose parameters have been calculated by means of the Least Square Method (LSM). The Mean temperatures, the Fractiles 2 % and 98 % and the Correlation Coefficients are also given in the same figures and collected in Table 1 also for the other investigated months.

It can be noticed that Normal Distribution exhibits systematically the best correlation coefficients and therefore the *Gaussian* PDF has been selected as the most suitable to study the statistical properties of all the collected monthly random samples.

The diagrams of fig. 4 and 5 respectively contain the just-as-sampled temperature measures of sensors 67 and 105. Mean temperatures, 2 % and 98 % fractiles of each mean monthly day have been also plotted versus a central day of the month while intermediate values have been obtained by means of linear interpolation.

A first remark concerns the amplitude of the confidence interval which is evidently larger in Winter than in Summer, particularly for sensor 67 which is close to the outer surface. Although being a completely different type of structure, the prestressed concrete box girder bridge Casilina exhibited the same property [6]. It can therefore be argued that, independently from the struc-

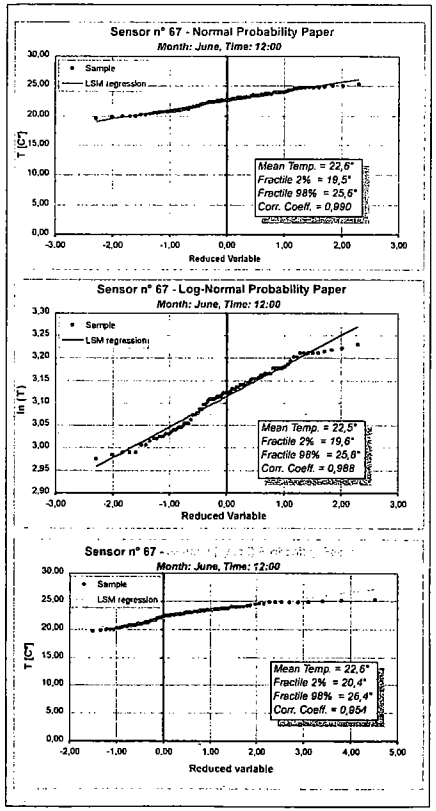

Fig. 2. Sensor 67: Gaussian, Log-normal and Gumbel PDF plotted on probability papers for the month of June
Bild 2. Sensor 67: Gauß-, Log-Normal- und Gumbel-Verteilung auf logarithmischem Papier für den Monat Juni

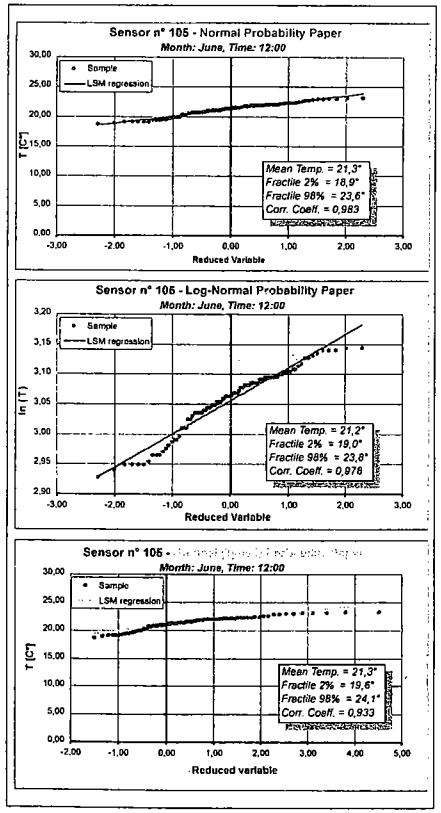

Fig. 3. Sensor 105: Gaussian, Log-normal and Gumbel PDF plotted on probability papers for the month of June
Bild 3. Sensor 105: Probabilistische Dichtefunktion für den Monat Juni

tural type, the greater dispersion of winter temperature data depends only on the weather features of Central Italy which have in Winter a greater instability degree than in Summer.

This is confirmed also by the correlation coefficients which are always greater in June than in all the other three observed months (see Table 1) independently on the chosen PDF.

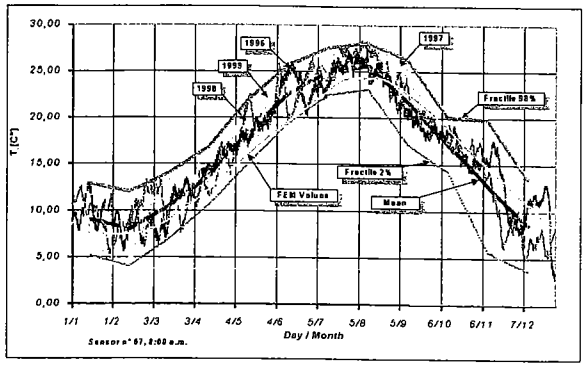

Fig. 4. Sensor 67: Just-as-sampled daily temperatures, mean temperatures, fractiles 2 % and 98 %, FEM values
Bild 4. Sensor 67: FEM-Werte, 2 %- und 98 %-Fraktile der Haupttemperaturen

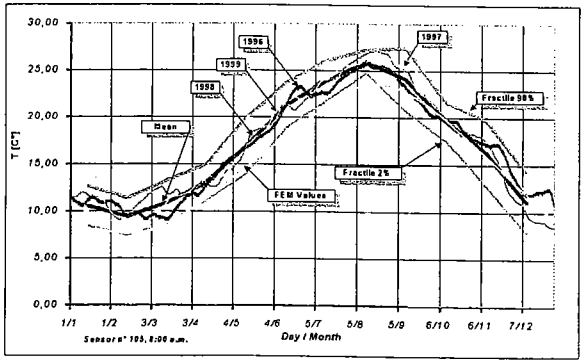

Fig. 5. Sensor 105: Just-as-sampled daily temperatures, mean temperatures, fractiles 2 % and 98 %, FEM values
Bild 5. Sensor 105: FEM-Werte, 2 %- und 98 %-Fraktile der Haupttemperaturen

4 Comparison of temperature measurements with FEM values

The comparison between theoretically predicted and statistically analysed temperature values must be conveniently performed under the two aspects of the time and the space variation.

Fig. 4 and 5 emphasise the time comparison evidencing quite a good annual phase matching between theoretical calculated values and the correspondent experimental measures at the selected instant (8.00 a.m.). A satisfactory phase coincidence is achieved also in the daily period as evidenced in fig. 6 to 9 which reproduce the temperature distributions within the thickness of the masonry at the same instants (8.00 a.m.) of the solstice days. Analogous distributions, related to other instants can be found in reference [7].

It can be observed that temperatures are somewhat generally underestimated in the Spring–Summer period where the maximum error is about 4 °C, as if there would be a input lack of direct solar radiation in the modelled boundary conditions. This could be found rather surprising since fig. 1 shows that both instrumented holes come next to outer surfaces which are prevalently shadowed by the lodges. But looking at the same figure, it can also be noticed that these two sensors are probably reached by a descending heat flux induced at the round walks surfaces by the direct solar radiation, here acting quasi perpendicularly, which has been neglected in the 2D model.

Nevertheless, calculated values are as a whole almost every time comprised within the confidence region; the annual average divergence between experimental mean values and FEM values is just about 2 °C while in the Autumn–Winter period the approximation is really satisfactory.

Table 1. Cumulative distribution function
Tabelle 1. Kummulative Verteilungsfunktion

			Cumulative Distribution Function											
			Normal				Log-Normal				Gumbel (Type I)			
Sensor N°	Orientation	Month	Mean value [C°]	Fractile 2% [C°]	Fractile 98% [C°]	Corr. Coeff.	Mean value [C°]	Fractile 2% [C°]	Fractile 98% [C°]	Corr. Coeff.	Mean value [C°]	Fractile 2% [C°]	Fractile 98% [C°]	Corr. Coeff.
67	North	March	10,4	6,9	13,8	0,970	10,2	7,2	14,6	0,955	10,4	7,9	14,5	0,907
		June	22,6	19,5	25,6	0,990	22,5	19,6	25,8	0,988	22,6	20,4	26,4	0,954
		September	21,6	17,1	26,2	0,971	21,5	17,4	26,6	0,971	21,6	18,4	27,3	0,935
		December	8,5	3,6	13,3	0,993	8,1	4,3	15,3	0,965	8,5	5,0	14,4	0,951
105	South	March	10,9	8,6	13,2	0,953	10,8	8,8	13,4	0,948	10,9	9,3	13,7	0,899
		June	21,3	18,9	23,6	0,983	21,2	19,0	23,8	0,978	21,3	19,6	24,1	0,933
		September	24,0	20,7	27,4	0,953	24,0	20,8	27,6	0,949	24,0	21,7	28,0	0,880
		December	11,1	8,1	14,1	0,938	11,0	8,2	14,7	0,901	11,1	9,0	14,7	0,867

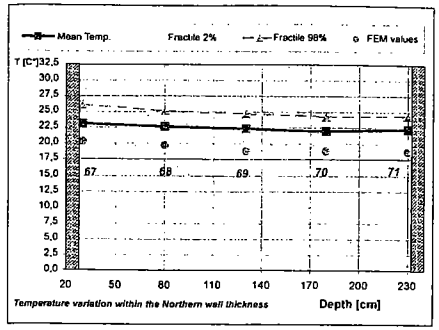

Fig. 6. Temperature variation across the northern wall (21st June)
Bild 6. Temperaturänderungen in der Dicke der nördlichen Wand (21. Juni)

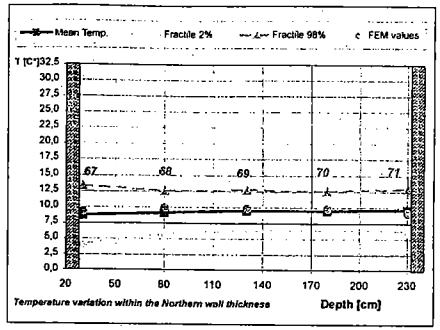

Fig. 7. Temperature variation across the northern wall (21st December)
Bild 7. Temperaturänderungen in der Dicke der nördlichen Wand (21. Dezember)

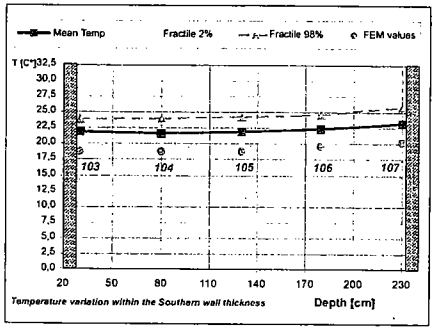

Fig. 8. Temperature variation across the southern wall (21st June)
Bild 8. Temperaturänderungen in der Dicke der südlichen Wand (21. Juni)

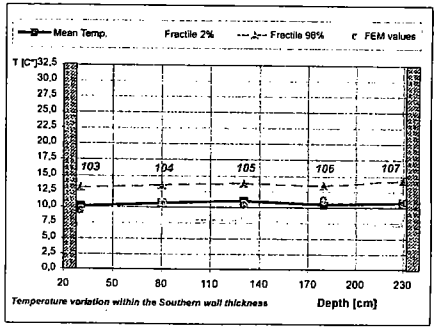

Fig. 9. Temperature variation across the southern wall (21st December)
Bild 9. Temperaturänderungen in der Dicke der südlichen Wand (21. Dezember)

5 Conclusions

In spite of the large number of simplifying assumptions assumed in the FEM model and the uncertainties and approximations with which the boundary conditions have been defined just from literature climatic data (see [4]), predicted temperatures resemble satisfactory well experiments under both the aspects of the time and the space variations. This confirms that sufficiently accurate estimations of the thermal behaviour of even complex shaped ancient masonry buildings can be performed for structural purposes just by means of relatively simple modelling.

Of course, also residual discrepancies between theory and measures could be minimised at will in the future by improving the geometrical refines of the model, by better defining the boundary conditions directly using in situ measured climatic data and by identifying **a posteriori** unknown or uncertain quantities like the coefficients of convection heat exchange by means of retrofitting operations.

Acknowledgements
The writers would like to express their deep gratitude to Prof. *M. Jamiolkowski*, co-ordinator of the Comitato Internazionale per la salvaguardia della Torre di Pisa who authorised the transmission of the temperature measurements and to Ing. *P. Heiniger*, director of the Tower workshop, who materially supplied the data.

A particular thank to the students, candidate engineers, *G. Azzone* and *M. G. Bevilacqua* who skilfully and patiently helped the authors in the work of organising the data files and of drawing some figures.

References

[1] *Noccioli, R., Polvani, G., Salvioni, G.*: I movimenti della torre dal giugno 1911 a tutto il 1968. Ricerche e Studi su la Torre Pendente di Pisa e i fenomeni connessi alle condizioni d'ambiente. Rapporto N° 3, Vol. I, pgs. 97–150. Ministero dei Lavori Pubblici, Commissione per il Consolidamento della Torre pendente di Pisa (legge 19 maggio 1965, N° 506). Istituto Geografico Militare, Firenze, 1971.

[2] *Burland, J. B., Viggiani, C.*: Osservazioni sul comportamento della Torre di Pisa. Rivista Italiana di Geotecnica, N° 3, pgs. 179–200, 1994.

[3] *Camuffo, D.* et al.: Studio di analisi del microclima e delle interazioni ambiente-manufatto. Rapporto interno, Comitato Internazionale per la Salvaguardia della Torre di Pisa, 1995.

[4] *Froli, M., Ulivieri, E.*: Transient Temperature Fields and Thermal Actions in the Leaning Tower of Pisa. Bautechnik, Vol. 78 (2001), N° 5, pgs. 348–361.

[5] Consiglio Nazionale delle Ricerche: Dati climatici per la progettazione edile ed impiantistica. Roma, 1982.

[6] *Barsotti, R., Froli, M.*: Statistical Analysis of Thermal Actions on a Concrete Segmental box-Girder Bridge. Structural Engineering International, N° 2, pgs. 111–116, 2000.

[7] *Froli, M., Formichi, P.*: A Comparison between Theoretical Predictions and Statistical Analysis of Temperatures Measurements in the Leaning Tower of Pisa. Rapporti di Studi e Ricerche del Dipartimento di Ingegneria Strutturale dell'Università di Pisa, N° 9, 2002.

Authors of this paper:
Prof. Ing. Maurizio Froli, Dr.-Ing. Paolo Formichi, Dipartimento di Ingegneria Strutturale dell'Università di Pisa, Via Diotisalvi 2, I – 56126 Pisa

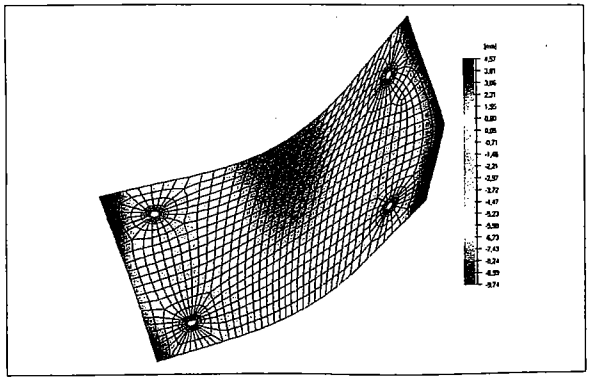

Verlauf der Verformung bei punktgehaltener Verglasung

DOI: 10.1002/bate.200610004

Maurizio Froli
Enrico Ulivieri

The Calculation of Thermal Movements and Eigenstresses in the Leaning Tower of Pisa

Starting from predicted yearly and daily distributions of the temperature fields induced by climatic actions over the cross-sections of the Leaning Tower of Pisa, the correlated time histories of thermal movements and eigenstresses have been calculated by simply assimilating the monument to a prismatic, inhomogeneous elastic body. Comparisons performed between calculated and measured daily and seasonal thermal displacements evidenced a good prediction capability of the model and its attitude to be used as an interpretation tool to understand also thermal periodical movements in other tower-shaped buildings.

Die Berechnung thermischer Bewegungen und Eigenspannungen am Schiefen Turm von Pisa. *Ausgehend von den prognostizierten jährlichen bzw. täglichen Temperaturfeldverteilungen, die durch klimatische Einwirkungen über die Querschnitte des Schiefen Turms von Pisa entstehen, sind korrelierte Time-history-Modelle der thermischen Bewegungen und der Eigenspannungen berechnet worden, wobei der Turm näherungsweise als einfacher prismatischer, inhomogener elastischer Körper aufgefaßt wird. Vergleiche zwischen berechneten und gemessenen täglichen und jahreszeitlichen thermischen Verschiebungen ergaben gute Übereinstimmung und machen durch die gute Prognose-Kapazität das Modell zu einem Interpretationstool für das Verständnis der periodischen thermischen Bewegungen auch vergleichbarer anderer Bauwerke.*

1 Introduction

Many special structural problems are originated in masonry buildings by complex and often reciprocally coupled phenomena of heat propagation and humidity diffusion caused in most cases by the interaction between the structure and its surrounding environment. Normally only serviceability problems arise, like minor cracking, but in some cases thermal gradients activate also the propagation and diffusion of aggressive substances, like water and CO_2, thus leading to important degradation of the mechanical resources of the material and also, in some cases, to a severe risk for the global structural safety (*Bažant e Ferretti* [1]). In order to better understand and to face these problems, structural engineers have been compelled to turn their attention also to the calculation and prediction of thermal fields in order to achieve the initial input data set necessary to go forth with calculating related movements and stresses.

It is well known that non-uniform and non-stationary temperature distributions may be induced in building structures not only by climatic agents but also by service conditions, as in cryogenic storage tanks, or by internal heat sources, as typically in fresh poured concrete casts. However, complex heat exchanges always occur at the exposed surfaces between the structure itself and the climatic environment which have to be considered if realistic descriptions of these thermal fields are required [2]. This preliminary problem has already been discussed in a precedent paper for the case study of the Leaning Tower of Pisa, where a simplified geometrical model of the monument, including also shadow effects, was used to calculate at any internal point the complete daily and annual time history of the temperature fields [3].

We just recall here that the Leaning Tower was ideally schematised as the coaxial superimposition of two smooth circular, hollow cylinders – the basement and the shaft – where the heat flux parallel to the structure axis was supposed negligible. Each marble column of the six lodges was also singularly analysed as an isolated solid cylinder exerting no thermal interaction with the lodges and with the shaft, except that of reciprocal shadowing. This simplified thermal model was later validated in a comparative investigation [4], where the predicted mean temperature fields satisfactory matched the statistically processed population of the available temperature measurements. This result allowed to prosecute, with the present paper, namely the study of the mathematical prediction of the movements and of the eigenstresses induced by the climate in the Tower.

2. The mechanical model

2.1 Basic geometrical and structural hypotheses

To calculate the mechanical effects induced in the Tower by the previously calculated thermal fields it was decided, for sake of uniformity, to follow the same idea of model simplicity adopted also in the precedent thermal analysis and not to adopt a fine meshed, 3D FEM model with a large number of solid elements like that, for example, used by *Viskovic* and others [5] for the same purpose. Another reason for such a methodological choice was the desire of enucleating in the most clear and evident way just the major and dominant aspects of the thermal behaviour of the monument. Aspects which only a compact model is able to emphasize.

As far as the geometrical aspect is concerned, the mechanical model of the Tower does not differ at all from the

thermal one. As illustrated in figure 1a, it consists of a first long cylinder, the shaft, coaxially laid upon another shorter but broader one, the basement. The six lodges are schematised by six circular tora with rectangular cross sections and enclosed at each loggia by thirty columns, which are assimilated to straight cylinders. The belfry, although sketched in fig.1, is not part of the model. From the mechanical point of view, both the basement and the shaft are considered like elastic beams connected in series. The cross section of the basement is composed by three concentric heterogeneous circular coronas of which the two outermost schematise the marble facings while the intermediate reproduces the infill masonry. The cross section of the shaft has the same inner diameter of the basement, a smaller outer diameter and the same sequence of outer marble facings and infill masonry. The presence of the stair case void has been neglected too. In the calculations, each column is thought as being connected in parallel with the shaft itself by means of the lodges (see [3], figs. 3a, 3b) and not being able to transmit bending moments. Accordingly the cross section of all the columns can be considered part of the cross section of the shaft. The disks schematising the lodges have been supposed perfectly rigid and the cross sections of the basement and of the shaft to remain plane (*Bernoulli-Navier* hypothesis).

The search for the most appropriate values of the *Young*'s modula E_1 and E_2 and of the coefficients of thermal expansion α_1 and α_2 , respectively of the San Giuliano marble external facings and of the infill masonry, has constituted a crucial step in the calculations. Indeed it significantly influences the prediction accuracy of the method since the definition of synthesis quantities as the Effective Mean Temperature (E.M.T. or T_m) and the Effective Global Linear Gradients (E.G.L.G. or DT_x and DT_y) is based on a mechanical and thermal homogenisation procedure performed with the help of ratios $n_E = E_1 / E_2$ and $n_\alpha = \alpha_1 / \alpha_2$ (see [4], relations (8), (9), (10)).

On the other hand, it has already been remarked [3] that available, directly measured data on the elastic modula of the two materials are scarce and their values rather scattered. First rough measurements of the *Young*'s compression modulus of San Giuliano marble (E_1) were performed in 1913 (see: [6], Vol. I, Rapporto N° 1, pgs. 55-56) on three prismatic specimens. In 1971 more refined tests were performed on four 70 × 70 × 300 mm specimens which gave values comprised between 79101 and 74035 MPa with a mean value of 76373 MPa; no measurement of the infill modulus (E_2) was executed. Similar tests were performed in 1986 and in 1987 at the University of Pisa [7] and in 1987 also in Bergamo at the ISMES Laboratory [8] on ∅ = 54 mm cylindrical drilled samples of San Giuliano marble and of infill masonry specimens too. Other values of E_1 and E_2 have been obtained respectively by means of flat jack and borehole jack testing instruments [10]. All the Pisa and Bergamo results were comprised between 104300 and 72700MPa for the marble and between 27610 and 7260 MPa for the infill masonry (see Table 1, part a)). The wide range of the E_1 and E_2 experimental data is reflected in literature by the variety of values chosen by authors who tried to calculate stresses and displacements in the Tower (see Table 1, part b)). *Bartelletti* and *Selleri* [9] adopted for example E_1 = 78000 MPa and E_2 = 20000 MPa while *Jamiolkowski* and *Viggiani* [11] indicated for E_1 and E_2 possible variation ranges respectively comprised between 90000 and 70000 MPa and between

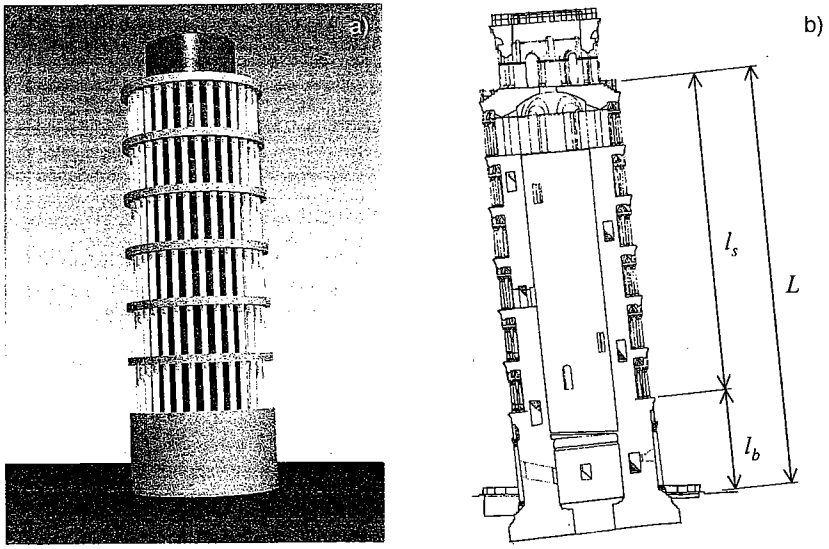

Fig. 1. External geometric shape of the mechanical model of the Tower as an assemblage of series and parallel connected straight circular hollow cylinders (a), vertical cross section (b)
Bild 1. Geometrische Daten des mechanischen Modells des Turms als seriell und parallel verbundene gerade Hohlzylinder (a), Längsschnitt (b)

Table 1. Literature data of the Young's modula of the S.Giuliano marble and of the infill masonry: a) available experimental measurements, b) values adopted or suggested by different authors
Tabelle 1. Zusammenstellung der E-Moduli von S. Giuliano-Marmor und dem Füll-Mauerwerk, a) vorhandene experimentell bestimmte Daten, b) Vorschläge verschiedener Autoren

	E_1 [MPa] (San Giuliano marble facings)			E_2 [MPa] (Infill masonry)			$n_E = E_1 / E_2$			
	Max	Min	Mean	Max	Min	Mean	Max	Min	Mean	Source
a) Experimental values	90200	79500	84000	–	–	–	–	–	–	[6] (1913)
	79101	74035	76373	–	–	–	–	–	–	[6] (1971)
	104300	72700	87950	12000	2900	7260	~ 36	~ 6	~ 12	[7] (1986)
	–	–	79780	–	–	27610	–	–	~ 3	[8] (1987)
	–	–	50000	–	–	7000	–	–	~ 7	[10] (1992)
b) Theoretical	–	–	78000	–	–	20000	–	–	~ 4	[9] (1976)
	90000	70000	–	7500	5000	–	18	9	–	[11] (1991)
	–	–	210000	–	–	70000	–	–	3	[5] (1997)

Table 2. Adopted ranges of the elasticity modula, of the thermal expansion coefficients and of the mechanical and thermal homogenisation coefficients
Tabelle 2. Zusammenstellung der Materialdaten

E_1 [MPa]	E_2 [MPa]	α_1 [°C^{-1}]	α_2 [°C^{-1}]	$n_E = E_1/E_2$	$n_\alpha = \alpha_1/\alpha_2$
27610	6150	$3.7 \cdot 10^{-6}$	$7.0 \cdot 10^{-6}$	27610/6150 ≅ 4	3.7/7.0 ≅ 0.5
104300	7260	$7.0 \cdot 10^{-6}$	$5.5 \cdot 10^{-6}$	104300/7260 ≅ 14	7.0/5.5 ≅ 1.27

7500 and 5000 MPa which appears very reasonable. As a matter of fact, borehole jack testing evidenced values of E_2 of about 7000 MPa which approach in our opinion rather realistically the actual bulk modulus of the infill masonry that has a porous structure, uniformly pervaded by voids of different size. For what E_1 is concerned, we must observe that, although their surfaces appears as compact masonry curtains composed by perfectly cut square stones with few millimetres thick contact joints, the external facings cannot be considered like completely homogeneous walls since the contact zone is very small, the inner parts of the marble ashlars are roughly wedge-shaped and penetrate in the infill for different depths (see [4], fig. 1). Therefore, the thickness of each facing must be taken as an average quantity including parts of the more compressible mortar. Consequently, an equivalent elasticity modulus of this composite material was estimated with the help of a convenient arrangement of series and parallel sets of marble and mortar parts schematising a facing sheet of sufficient length. These calculations gave equivalent $E_1 \cong 27000$ MPa. Therefore, assuming E_2 = 7260 MPa [7], the mechanical homogenisation coefficient n_E results to be about 4, in accordance with what indicated in [5] and [9]. In [10] the estimated possible variation interval of n_E is comprised between 4.5 and 16.7. Naturally, definitely reliable average values of E_1 and E_2 could be stated only by means of tests on sufficiently large pieces of masonry including parts of the external facings but it is obvious that such experiments are impracticable.

The search for appropriate values of the coefficients of thermal expansion of the marble (α_1) and of the infill masonry (α_2) was even more problematic since no direct measurements of these quantities have yet been performed

Table 3. Couples of mechanical and thermal homogenisation coefficients adopted in the calculations
Tabelle 3. Paarweise ausgewählte mechanische und thermische Koeffizienten, die für die Berechnung verwendet wurden

	$n_\alpha = 0.5$	$n_\alpha = 1.27$
$n_E = 4$	(a)	(b)
$n_E = 14$	(c)	(d)

and therefore just literature data related to similar materials had to be taken. *Camuffo* [12] assumes for San Giuliano marble $\alpha_1 = 8.0 \cdot 10^{-6}$ °C^{-1} like for a usual calcareous stone. Ordinary Carrara marble has $\alpha_1 = 6.3 \cdot 10^{-6}$ °C^{-1} but the quality Carrara Venato exhibits the lower value $\alpha_1 = 3.7 \cdot 10^{-6}$ °C^{-1} while, for example, the red Verona marble reaches $\alpha_1 = 9.40 \cdot 10^{-6}$ °C^{-1}. *Viskovic* and others [5] assume $\alpha_1 = 7.0 \cdot 10^{-6}$ °C^{-1} and for α_2 they take the same value of ordinary terracotta bricks: $\alpha_2 = 5.5 \cdot 10^{-6}$ °C^{-1}.

Table 2 collects the minimum and maximum values of the here assumed equivalent elasticity modula, thermal expansion coefficients and related mechanical and thermal homogenisation coefficients of the two materials. In order to cover all these uncertainties, movement calculations have been repeated for each of the four possible combinations of the minimum and maximum homogenisation coefficients gathered in table 3.

3 The calculation of movements

Since we have schematised the Tower as an assemblage of series and parallel connected straight circular hollow beams,

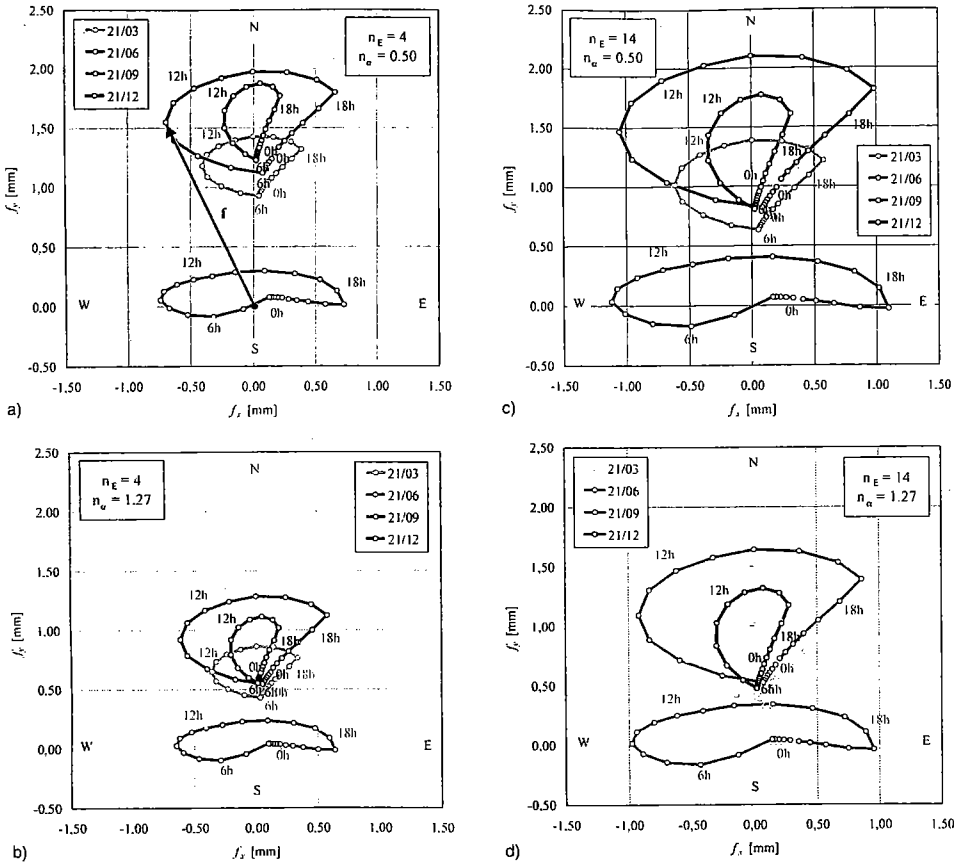

Figure 2. Daily trajectories of the Tower's top calculated for different values of the homogenisation coefficients n_E and n_α in correspondence of all the hours of the quadrant days (21th March, 21th June, 21th September, 21th December).
Bild 2. Trajektoren über den Tag am Turmkopf für verschiedene Werte der Homogenisierungskoeffizienten n_E and n_α

the calculation of the thermal displacements of its top, perpendicular to the axis, follows directly from the knowledge of the Effective Global Linear Gradients (E.G.L.G.). We calculate these movements starting from a purely ideal initial condition of a Tower free from any E.G.L.G., so that its longitudinal axis is not curved by temperature distributions.

In this ideal configuration of thermal rest let us place a reference system (x,O,y) in the plane of the uppermost cross section with the origin O in the centre of it and the x and y axis respectively coincident with the W-E and the S-N direction (fig. 2). We call the origin O point of theoretical thermal rest. If we now denote with DT_{bx}, DT_{by} the E.G.L.G. components along x and y acting at a certain instant in the basement and with DT_{sx} and DT_{sy} those acting in the shaft, the corresponding components f_x and f_y of the total displacement vector f are given by relations (1.1) and (1.2) where ℓ_b and ℓ_s are the lengths of the basement and of the shaft while L (46 m) is the total height of the Tower at the belfry level (Fig. 1b). The magnitude of f is of course given by

$$f = \sqrt{f_x^2 + f_y^2}$$

$$f_x = \frac{\alpha_2}{2}\left(DT_{sx}\ell_s^2 + DT_{bx}\ell_b(L + \ell_s)\right) \qquad (1.1)$$

$$f_y = \frac{\alpha_2}{2}\left(DT_{sy}\ell_s^2 + DT_{by}\ell_b(L + \ell_s)\right) \qquad (1.2)$$

The minus sign in relations (1.1) and (1.2) means that under positive gradients (northern side warmer than the southern one and oriental side warmer than the occidental one [3]), the displacements develop along the negative direction of respectively y and x axis, that is southwards and westwards. The E.M.T. produces a length variation of the tower axis which also produces displacement components along x and y. Their magnitude is however very small in comparison with those originated by gradient displacements and can be completely ignored.

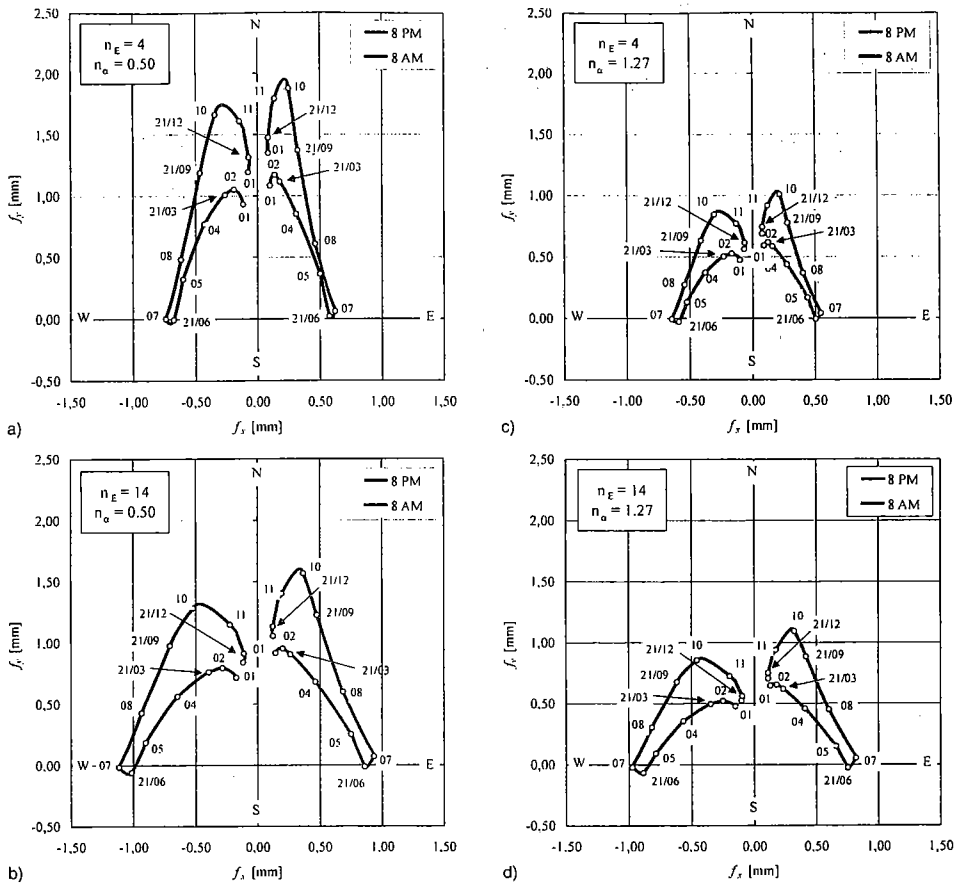

Figure 3. Yearly 8:00 and 20:00 h isochronous trajectories of the Tower's top calculated for different values of the homogenisation coefficients n_E and n_α in correspondence of the middle days of each month
Bild 3. Jährlicher Verlauf der isochronen Trajektorien am Turmkopf für verschiedene Werte der Homogenisierungskoeffizienten n_E and n_α

3.1 Daily movements

The daily developments of the total displacement vector f are represented by polar graphs in figures 2a and 2b, where the position of the Tower's top has been calculated at each hour of the quadrant days (summer and winter solstices, spring and autumn equinoxes). The calculations have been then repeated for all the chosen couples of mechanical and thermal homogenisation coefficients. All the graphs exhibit common features that do not depend on the choice of n_E and n_α. Different choices of the homogenisation coefficients produce only scale expansions or contractions of the curves.

Diurnal trajectories are clearly distinguished from the night paths in that, during the day the top of the Tower covers a sort of elliptic trajectory, always in opposition to the apparent motion of the sun across the sky, as though the monument would try to escape the direct radiation of the star. During the night hours, regardless of the season, the cooling down process progressively reduces the E.G.L.G. components and the top of the Tower approaches point O. The great thermal inertia of the fabric would require a longer time to completely extinguish the residual E.G.L.G. components before the next sunrise. Therefore all the night trajectories converge towards the point of thermal rest without succeeding in reaching it. Only if night conditions would ideally persist without interruptions for many consecutive days the Tower would steadily reach its position of theoretical thermal rest.

Two consecutive points in the graphs of figure 2 are separated by a time interval of one hour. Therefore their reciprocal distance is inversely proportional to the displacement velocity. We can observe that the daily quickest movements (~ 0.25 mm/h) are performed in the East-West direction both in the morning and in the afternoon of June

or September days while during the night the Tower slows more and more down towards point O. All the year long the thermal movements take place northern to point O meaning that the Tower's axis is almost always curved by solar radiation in opposition to the leaning induced by soil settlements which is, as known, directed southwards. Only the June trajectory, which is the southernmost one, intercepts point O at the beginning of the day. During the subsequent morning hours even negative values of f_y can be observed that are in the same direction of the geotechnical leaning, but they rapidly disappear as soon as the sun approaches the position of zero azimuth at 12:00 h.

It seems than as if the Tower, although forced by some evil force to lean but still free to choose the direction, might have chosen the less unfavourable one. In June the top covers the largest range in the East-West direction and the shortest one in the South-North direction. This can be explained by the fact that the sun rays hit the outer surfaces both in the morning and in the afternoon at angles near 90° while they are almost parallel to the axis around midday, helped also by the natural leaning. In September the daily East-West range is comparable to the South-North range while in a December day the top moves practically almost in the meridian direction since the sun radiation, although weaker than in June, is around 12:00h almost perpendicular to the outer surfaces.

3.2 Simple and double periodicity of the yearly movements

Eloquent pictures of the annual movements can be obtained by drawing in the same reference system of figures 2 all the positions assumed by the Tower's summit in correspondence of a selected hour for all the days of the year. Figures 3a–d collect, for example, all the points calculated at 8:00h and at 20:00h of the middle day of each month. Such isochronous trajectories can of course be traced for any other hour of the day. As for the graphs of figure 2, also these calculations have been repeated for the four selected combinations of n_E and n_α.

Let us consider any one of these diagrams, for example that of figure 3a, and let us look in particular at the annual trajectory of the 8:00 hours. We observe first of all that in the morning the top of the Tower is always located in the N-W quadrant ($f_x < 0$, $f_y > 0$) except, as already evidenced, for the short period between June and July where it invades also a little portion of the S-W quadrant ($f_x < 0$, $f_y > 0$). The periods around the solstice days delimitate two different arched trajectories of similar shape that could be almost reciprocally derived from each other by suitable simple deformations and translations.

It is quite remarkable that in correspondence of summer and winter solstices there is an inversion both in the Eastwards and in the Northwards displacements, while during the days around February and around the beginning of November inversions take place only in the Northwards displacements. Eastwards displacements have therefore a simple yearly periodicity since they exhibit a constant monthly increase in the first interval (January – to June/July) and a constant monthly decrease in the second interval (June/July – to January). On the other hand, northwards movements have a double periodicity over the year, since they increase from January until February, decrease from February until June, grow up again until the first days of November and then decrease again till January. This fact is

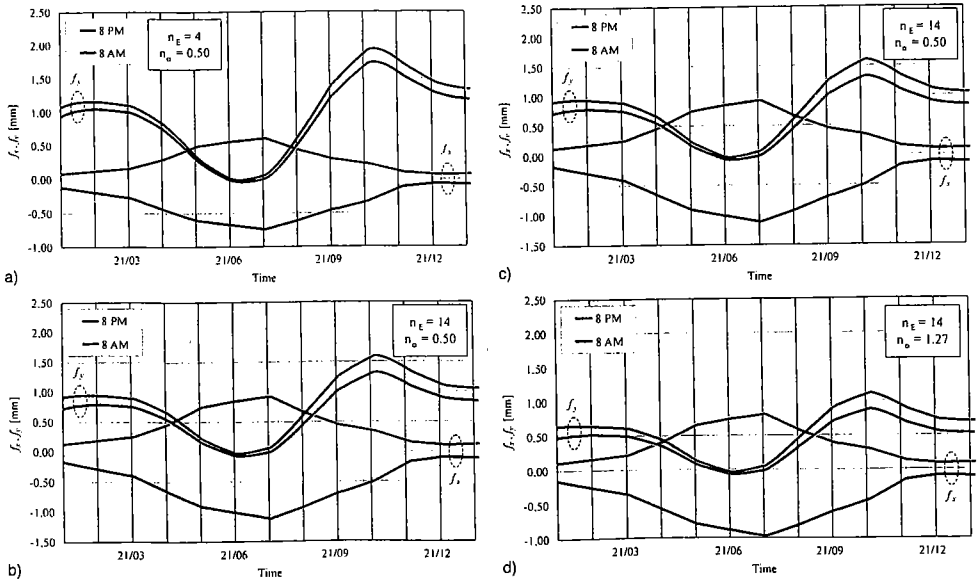

Figure 4. Yearly distributions of f_x and f_y components calculated at 8:00 and 20:00 h of the middle days of each month
Bild 4. Jährlicher Verlauf der f_x- und f_y-Komponenten

clearly evidenced in fig. 4 where the f_x and f_y components are separately plotted versus the months of the year.
The model is therefore suitable for reproducing and explaining the famous phenomenon that puzzled experts for so many years until now, of the observed simple and double yearly periodicity of thermal movements along respectively the W-E and the N-S direction.
Qualitative identical behaviours can be obtained by drawing other isochronous trajectories. For example, if we look in the same figure 3a at the 20:00h trajectory, we observe that it is qualitatively specular to that of 8:00h and that analogous considerations apply.

3.3 The point of thermal rest – comparison between predicted and measured daily thermal movements

The existence of thermal movements was for the first time experimentally evidenced when *Girometti* and *Bonechi* installed on 1st September 1934 their 30 m long, 150 kgs heavy G.M. pendulum inside the internal void of the shaft where a condition of complete sheltering from the environmental disturbances was assured allowing the long pendulum to measure inclination variations with the precision of (0",01. Since the magnitude of the annual slope increase due to soil settlement before the stabilization works of 1999 was about 5", the daily slope increment of geotechnical origin should have been consequently comparable to the instrument's error and almost invisible but nevertheless hourly records of the pendulum positions evidenced a sort of cyclic movement with a amplitude of about 3" ÷ 5". It was immediately clear that the Tower's top performed such movements during the course of each day under the influence of sun radiation and of the other climatic agents (see: [6], Vol. I, Report N° 3, Chapt. I., § 6.3). Thermal movements began than to be periodically controlled in order to clean up from them geodesic measurements.

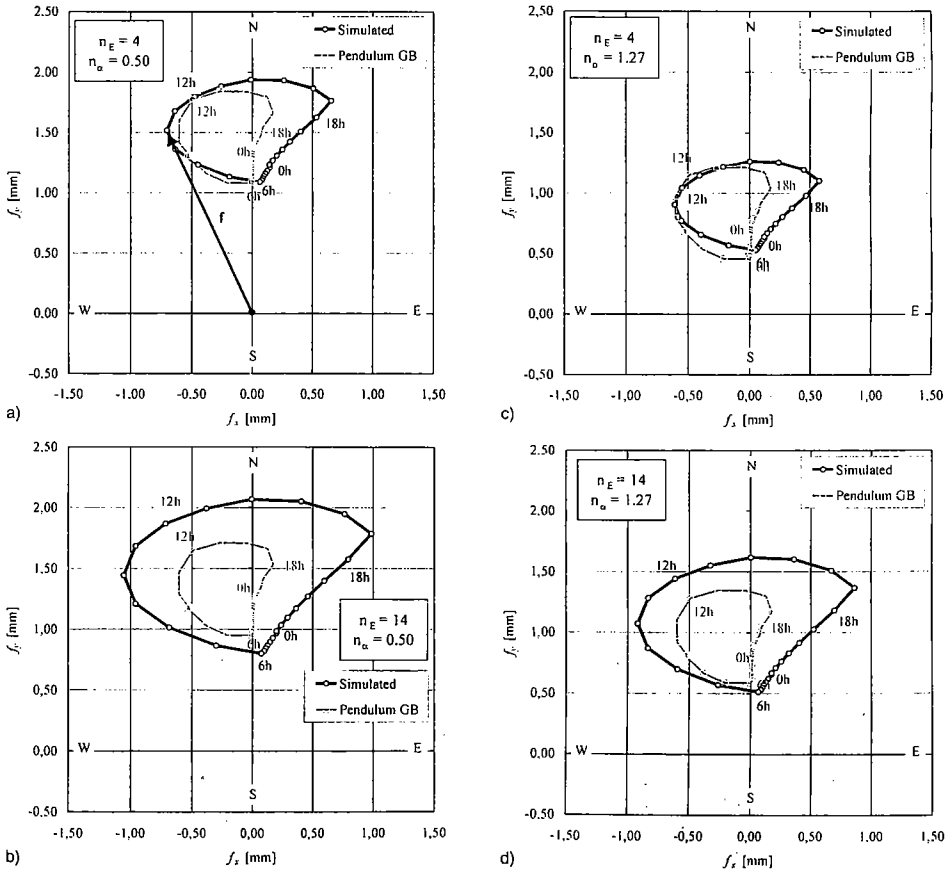

Figure 5. Comparison of the daily trajectories of the Tower's top calculated for different values of the homogenisation coefficients n_E and n_α and the trajectory measured by the G.B. Pendulum in correspondence of a September day
Bild 5. Vergleich der Tagestrajektorien am Turmkopf für verschiedene Werte der Homogenisierungskoeffizienten n_E and n_α und der Trajektorien aus dem Pendelversuch an einem Septembertag

We have found that components f_x and f_y of thermal movement must be referred to the point O of thermal rest but this concept was ignored until now and of course nobody has ever thought to research its location. As a consequence, G.B. daily thermal movements have been systematically drawn on graphs referred to arbitrary chosen origin points usually approximately coincident with the centroid of each quasi closed daily trajectory. For this reason direct comparisons between calculated and available measurements of daily thermal displacements are not immediately executable. To do that, it is first of all necessary to extrapolate the position of the experimental point O of thermal rest and let it coincide with the theoretical one deduced for each combination of the homogenisation coefficients n_E and n_α. figures 5a–d collects these results for September conditions. It can be seen that the abscissus of experimental O can be easily estimated since the f_x components of the last night hours practically all lie on the N-S direction, i.e. the westward movement is extinguished. The location of the ordinate of experimental O is on the contrary afflicted by some uncertainties because, although the cooling process slows down more and more during the last night hours and the corresponding f_y components are almost constant, the Tower has not yet completed its southwards journey when the sun rises up again.

Nevertheless, the comparison shows that daily trajectories calculated for $n_E = 4$, $n_\alpha = 0.50$ (fig. 5a) and for $n_E = 4$, $n_\alpha = 1.27$ (fig. 5b) approximate the measured trajectory much better than those calculated for $n_E = 14$, $n_\alpha = 0.50$ (fig. 5c) and for $n_E = 14$, $n_\alpha = 1.27$ (fig. 5d). It can be deduced that, at least for the mechanical homogenisation coefficient, the choice of $n_E = 4$, already operated in [3] and [4] confirms its validity for the calculation of movements while the question about which value, between $n_\alpha = 0.50$ and $n_\alpha = 1.27$, is the closest to reality is left open and shall be solved in the next paragraph.

4 Elastic eigenstresses

Taking advantage of the simplifying hypotheses that cross sections remain plain, the annular disks of the lodges are rigid and that marble and infill masonry behave within the linear elastic domain under tensile and compressive efforts, eigenstresses can be immediately deduced by applying the *Timoshenko*'s method of strain suppression extended to the category of heterogeneous beams like the present mechanical model. Under these assumptions it is easy to find that eigenstresses in the marble facings (domains A_1' and A_1''), in the infill masonry (domain A_2) and in the i^{th} marble column (domain A_c) are respectively given by formulae (2.1), (2.2), (2.3) where T(x,y) is the temperature of a point in the infill or in the facings and $(\bar{T}/x_i, y_i)$ is the mean temperature of the i^{th} column.

$$\sigma_{z1} = E_1\alpha_2\left((T_m + DT_y y + DT_x x) - n_\alpha T(x, y)\right) \quad (2.1)$$

$$\sigma_{z2} = E_2\alpha_2\left((T_m + DT_y y + DT_x x) - T(x, y)\right) \quad (2.2)$$

$$\sigma_i = E_1\alpha_2\left((T_m + DT_y y_i + DT_x x_i) - n_\alpha \bar{T}(x_i, y_i)\right) \quad (2.3)$$

Of course the real picture of thermal eigenstresses induced by the climate in the structures of the Tower is much more complex than that given by the preceding formulae where, beyond all the geometrical simplifications, radial and circumferential stress components are neglected as well as the influence of nonlinear phenomena like creep and cracking. On the other hand, just in virtue of their simplicity, expressions (2.1) to (2.3) have in our opinion the quality to give a first order estimation of clear meaning for primary elastic eigenstresses caused by climate induced temperature fields in the Leaning Tower.

4.1 Eigenstresses in the basement

The diagrams of figure 6a and 6b reproduce the hourly distributions of thermal eigenstresses calculated, for $n_\alpha = 0.50$, in six points of the N-S diameter and in six points of the W-E diameter of the basement during the four quadrant days of the year. Precisely, the two outmost points of the external facing, the two innermost points of the internal facing and the two mean points of the infill masonry have been selected for each diameter. The diagrams of figure and 7a and 7b reproduce the same quantities for $n_\alpha = 1.27$.

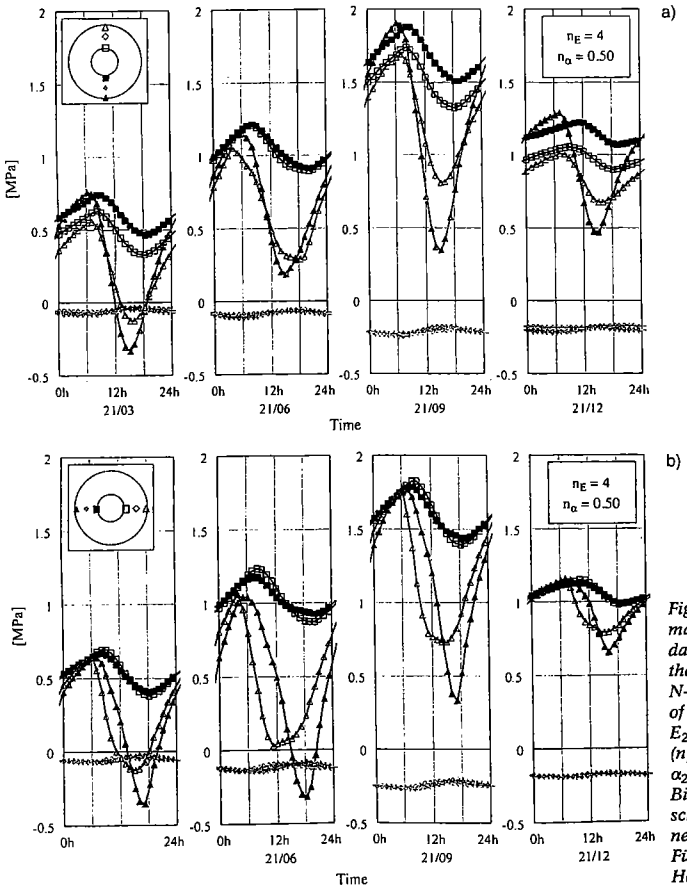

Figure 6. Hourly distributions of thermal eigenstresses, during the quadrant days, in some points of the facings and the infill masonry belonging to: a) the N-S diameter and b) the W-E diameter of the basement [E_1= 27610 MPa, E_2= 6150 MPa, ($n_E = 4$), $\alpha_1 = 3.5 \cdot 10^{-6}$ °C^{-1}, $\alpha_2 = 7.0 \cdot 10^{-6}$ °C^{-1}, ($n_\alpha = 0.50$)]
Bild 6. Stündlicher Verlauf der thermischen Eigenspannungen an verschiedenen Punkten der Fassade und des Füllmauerwerks für verschiedene Homogenisierungskoeffizienten

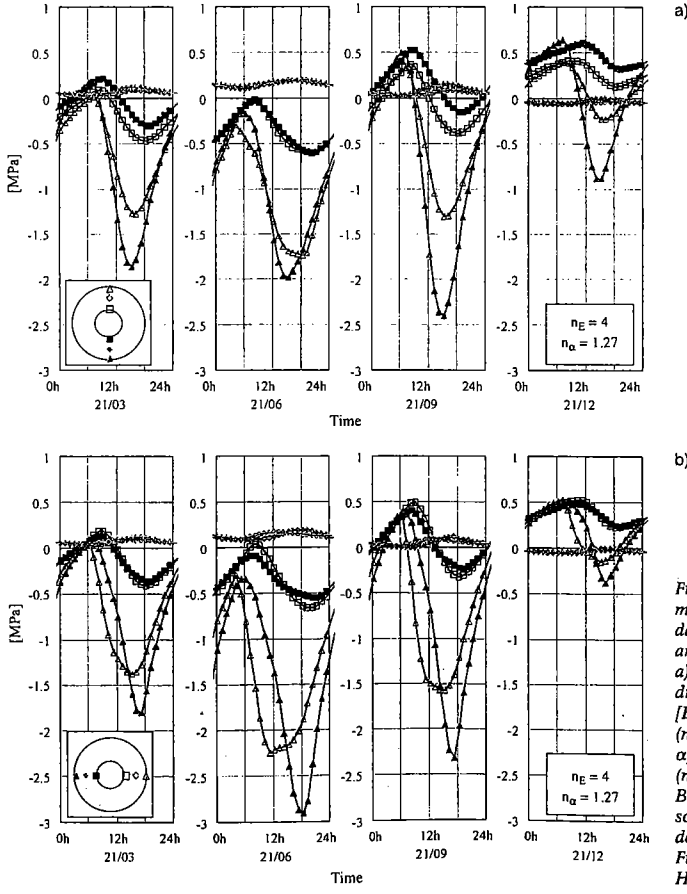

Figure 7. Hourly distributions of thermal eigenstresses, during the quadrant days, in some points of the facings and the infill masonry belonging to: a) the N-S diameter and b) the W-E diameter of the basement [E_1= 27610 MPa, E_2= 6150 MPa, ($n_E = 4$) $\alpha_1 = 7.0$ (10^{-6} °C^{-1}, $\alpha_2 = 5.5 \cdot 10^{-6}$ °C^{-1}, ($n_\alpha = 1.27$)]
Bild 7. Stündlicher Verlauf der thermischen Eigenspannungen an verschiedenen Punkten der Fassade und des Füllmauerwerks für verschiedene Homogenisierungskoeffizienten

4.1.1 Marble parts

If we compare the stress distributions of figure 6 to their correspondents of figure 7, it can be immediately seen that all the curves related to the marble parts have very similar shapes and almost superimpose one upon the other if conveniently shifted of a same constant quantity. In particular, if we assume $n_\alpha = 0.50$, we obtain everywhere tension stresses with the exception of the external facings during short time intervals in the afternoon of 21/03 and of 21/06. On the contrary, if we take $n_\alpha = 1.27$, the stress curves migrate downwards so that marble parts result prevalently compressed excepted the internal facings during the morning hours of 21/3, 21/9 and 21/12. All along the mean winter day both external and internal facings are tensioned excluded just some afternoon hours when the external facings are compressed. The sign inversion that follows the choice of n_α can be easily explained. We have already seen (figure 3) that the linear part of the thermal field, described by T_m, DT_x, DT_y and responsible of the movements, depends not much on the choice of n_E or n_α. Therefore, the prevalence in expressions (2.1) to (2.3) of the linear part of the temperature field on the punctual value of the temperature depends essentially on n_α; i.e., we get the plus or the minus sign respectively if the punctual temperature is reduced ($n_\alpha = 0.50$) or amplified ($n_\alpha = 1.27$) by the homogenisation factor.

From a physical point of view, compression eigenstresses in the most warmed up parts seem of course to have much more sense than tensile eigenstresses, also in accordance with other literature results ([5], [12]). Assumed $n_\alpha = 1.27$ as the most plausible thermal homogenisation coefficient, the maximum compressive stresses reach the intensity of almost 2.5 to 3 MPa in June and in September respectively in the easternmost and the southernmost point of the external facing. In September condition the biggest compressive oscillation (2.4 MPa) is also associated, in the same point, to the highest compression. It seems therefore probable that such high and frequent stress oscillation could induce, in the long period, to fatigue ruptures in the marble [13].

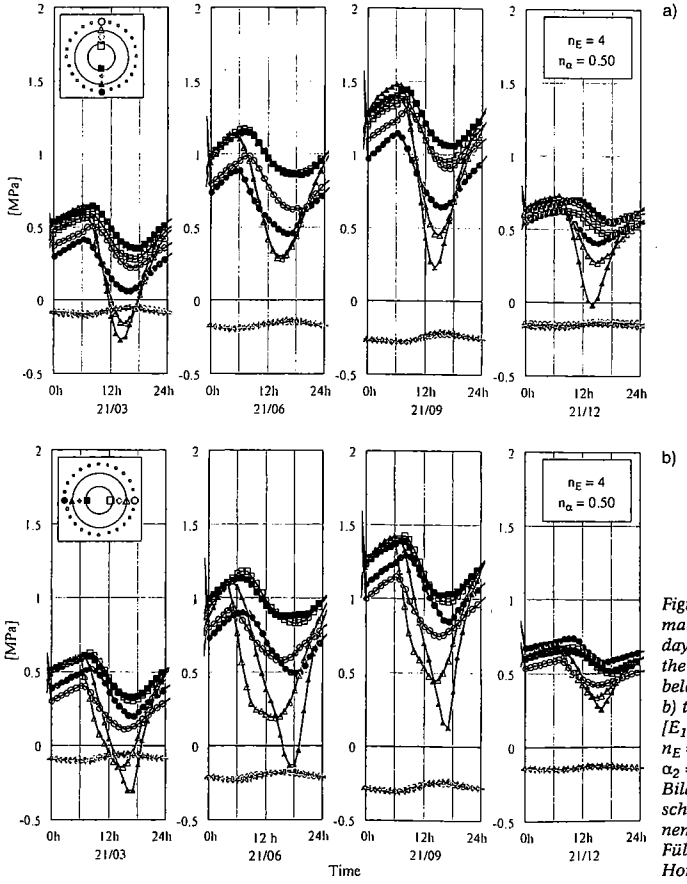

Figure 8. Hourly distributions of thermal eigenstresses, during the quadrant days, in some points of the facings, of the infill masonry and of the columns belonging to: a) the N-S diameter and: b) the W-E diameter of the shaft [E_1 = 27610 MPa, E_2 = 6150 MPa, $n_E = 4$), $\alpha_1 = 3.5 \cdot 10^{-6}\,°C^{-1}$, $\alpha_2 = 7.0 \cdot 10^{-6}\,°C^{-1}$, ($n_\alpha = 0.50$)]
Bild 8. Stündlicher Verlauf der thermischen Eigenspannungen an verschiedenen Punkten der Fassade und des Füllmauerwerks für verschiedene Homogenisierungskoeffizienten

4.1.2 Infill masonry

Eigenstresses in the infill of the basement are systematically opposite in sign with those in the facings and result greater in modulus when those in the facings are also greater, according to the condition of self-equilibrium. When stresses in the marble parts have a maximum they have always a minimum and vice-versa. Their intensities and daily oscillations are very low in comparison with those of the external parts, almost constant along the year and hardly any difference can be noticed during the same month between Western and Eastern or Northern and Southern points.

4.2 Eigenstresses in the shaft and in the columns

Eigenstresses in the facings and in the infill of the shaft have analogous time and space distributions as those in the basement. Intensities and daily oscillations are somewhat lower due to the shadowing effects of the lodges. Of particular interest are eigenstresses in the columns: their time distributions always well resemble those of the nearest facing but their intensities is systematically lower (1.2 MPa maximum compression stress) since in each column only instantaneous mean temperatures and not local peak temperatures have been considered. It is interesting to note that maximum gravity stresses were estimated by *Bartelletti* and *Selleri* as 3.5 MPa in the facings and 4.0 MPa in the columns.

5 Conclusions

The simple model of the prismatic, thermally inhomogeneous body which has been already successfully used to predict yearly and daily distributions of the temperature fields of climatic origin over the cross-sections of the Leaning Tower of Pisa, has been converted to a mechanically heterogeneous prism to calculate the time histories of thermal movements and eigenstresses in the monument. Comparisons performed between predicted and available experimental measurements of daily thermal movements have shown good accordance.

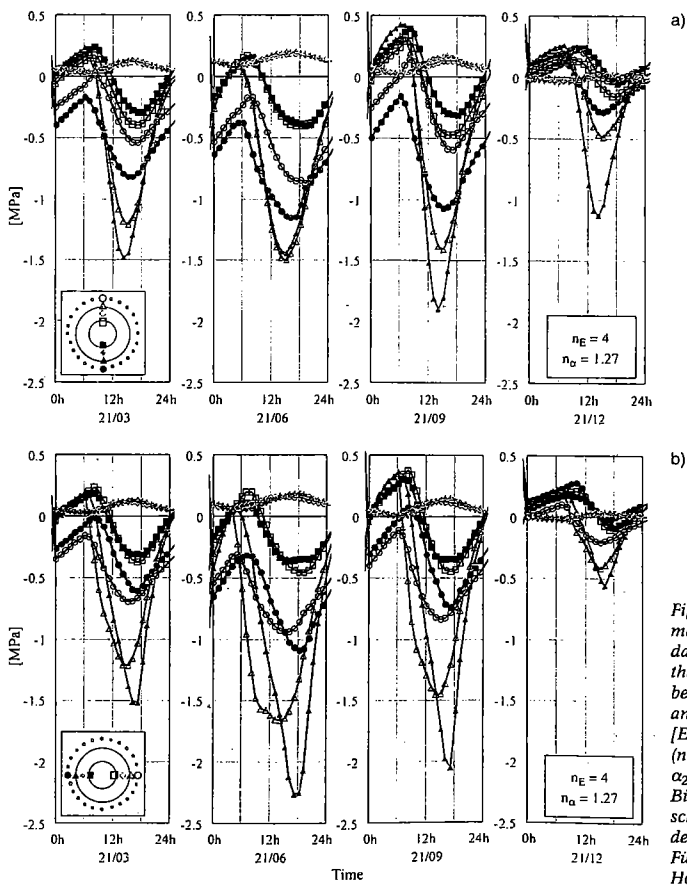

Figure 9. Hourly distributions of thermal eigenstresses, during the quadrant days, in some points of the facings, of the infill masonry and of the columns belonging to: (a) the N-S diameter and: (b) the W-E diameter of the shaft [E_1= 27610 MPa, E_2= 6150 MPa, ($n_E = 4$), $\alpha_1 = 7.0 \cdot 10^{-6}\,°C^{-1}$, $\alpha_2 = 5.5 \cdot 10^{-6}\,°C^{-1}$ ($n_\alpha = 1.27$)]
Bild 9. Stündlicher Verlauf der thermischen Eigenspannungen an verschiedenen Punkten der Fassade und des Füllmauerwerks für verschiedene Homogenisierungskoeffizienten

The model allowed also to simply explain the until now unsolved odd and puzzling phenomenon of the double yearly periodicity of the meridian thermal movements of the Tower and to introduce the concept of point of thermal rest that can be extended generally to all the tall, tower-shaped buildings.

Calculated elastic eigenstresses exhibit strong daily oscillations and reach maximum compression values of the same order of gravity induced compression stresses.

References

[1] *Bažant, Z.P., Ferretti, D.*, „Asymptotic temporal and spatial scaling of coupled creep, aging, diffusion and fracture processes", Creep, Shrinkage and Durability Mechanics of Concrete and other Quasi-Brittle Materials", CONCREEP 6, 2001, *F-J. Ulm, Z.P. Bažant* and *F.H. Wittman* eds., Amsterdam, Elsevier (invited lecture).

[2] *Froli M., Masiello G.*: „Transient Temperature Fields in Massive Concrete Castings interacting with the Environment during the Hydration Phase", L'Industria Italiana del Cemento, n° 797, April 2004.

[3] *Froli M., Ulivieri E.*: „Transient Temperature Fields and Thermal Actions in the Leaning Tower of Pisa", Bautechnik, 78 (2001), 5.

[4] *Froli M., Formichi P.*: „Statistical Analysis of Temperature Measurements in the Leaning Tower of Pisa in Comparison with Theoretical Predictions", Bautechnik, 79 (2002), 10.

[5] *Viskovic A., Carluccio G., Ambrosi A.*: „Verifica degli effetti delle variazioni termiche sullo stato di sollecitazione della Torre di Pisa", Prot. n°JAM 3750.58/tp, (Internal Report of the International Committee for the Safeguard and Stabilization of the Leaning Tower of Pisa), 1995.

[6] *Noccioli R., Polvani G., Salvioni G.*: „I movimenti della torre dal giugno 1911 a tutto il 1968", Ricerche e Studi su la Torre Pendente di Pisa e i fenomeni connessi alle condizioni d'ambiente", Ministero dei Lavori Pubblici, Commissione per il Consolidamento della Torre pendente di Pisa (legge 19 maggio 1965, n°506). Istituto Geografico Militare, Firenze, 1971.

[7] Istituto di Scienza delle Costruzioni dell'Università di Pisa (ISCUP) – Laboratorio Ufficiale per le Esperienze dei Materiali da Costruzione: Certificate n°656/86 and n°456/87, (ISCUP Internal Report), 1986, 1987, Pisa.

[8] ISMES: „Torre di Pisa – Determinazione di caratteristiche fisiche e di resistenza meccanica di campioni prelevati dalle murature della Torre", Prog.DGM/4136.A, Doc.REL/DGM/00135, Bergamo, 1987.

[9] *Bartelletti R., Selleri F.*: „Lo stato di tensione nelle strutture della Tore Pendente di Pisa", Atti dell'Istituto di Scienza delle Costruzioni dell'Università di Pisa, Vol.XVI, n°218, Pisa, 1978.

[10] *Calzona R., Creazza G., Croci G., Macchi G., Sanpaolesi L.*: „Structural Aspects", Proceedings of the Workshop on the Tower of Pisa, International Committee for the Safeguard and Stabilization of the Leaning Tower of Pisa, Opera della Primaziale Pisana, Quaderno n° 15, 1999.

[11] *Jamiolkowsky M., Viggiani C.*: „The Leaning Tower of Pisa – Present Situation", Proceedings of the X° European Conf. on S.M.F.E., 4: 1437-1445, Florence, 1991.

[12] *Camuffo D. et Al.* : „Torre di Pisa – Studio di analisi del microclima e delle interazioni ambiente-manufatto", Prot. n°JAM 3750.58/tp, Internal Report of the International Committee for the Safeguard and Stabilization of the Leaning Tower of Pisa, Padova Ricerche, 1995.

[13] *Cattaneo S., Labuz J.F.*: „Damage of Marble from cyclic Loading", ASCE J.Material of Civil Engineering, Vol.13, n°6, 2001.

Autors of these paper:

Prof. Ing. Maurizio Froli, Dipartimento di Ingegneria Strutturale dell'Università di Pisa, Via Diotisalvi, 2, I-56126 Pisa, Italy

Dr. Ing. Enrico Ulivieri, European Patent Office, D-80298 München

BAUTECHNIK aktuell

„Burj Dubai" – ein Turm in der Wüste

Im Dezember 2004 erteilte die Projektentwicklungsgesellschaft Emaar Properties einem internationalen Joint Venture, bestehend aus den Firmen Samsung Corporation (Süd Korea), Besix (VAE/Belgien) und Arabtec (Dubai) unter dem Projektmanagement von Turner Construction International den Auftrag zur Errichtung des höchsten Bauwerkes der Welt in Dubai.

Zentral in einem neuen Stadtteil inmitten eines künstlichen Sees entsteht das einer Wüstenblume nachempfundene 154 Stockwerk hohe Gebäude. Der Burj Dubai-Tower wird nach seiner Fertigstellung eine Nutzfläche von mehr als 4,2 Mio. m² für das erste Armani-Luxushotel, für exklusive Appartements, Büros sowie Einkaufs- und Dienstleistungszentren bereitstellen.

Das bauausführende Joint Venture hatte vor allem die Aufgabe zu lösen, den äußerst engen Zeitrahmen einzuhalten, bei dem alle drei Tage eine neue Decke geschalt werden muß. Gesucht wurde ein schnelles und hochleistungsfähiges Deckenschalungssystem.

Beim Burj Dubai-Tower kommt eine Kombination aus MevaDec-Standard- und -Sonderelementen zum Einsatz. Das ermöglicht die unkomplizierte Anpassung an die variierenden Grundrisse des sich nach oben verjüngenden Bauwerks.

Nach seiner Fertigstellung wird der Burj Dubai-Tower voraussichtlich über 800 m hoch sein. Genaue Angaben zur endgültigen Höhe werden z. Z. nicht gemacht.

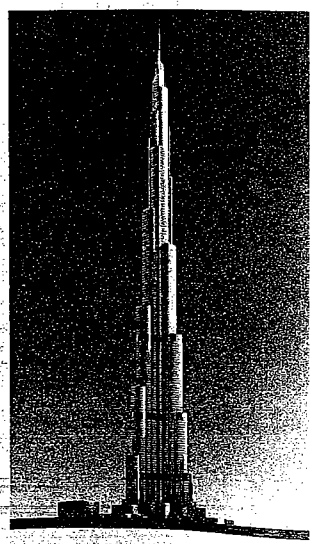

[Grafik: Getty Images Publicity, Business Wire]